V.V.Novikov, Yu.V.Nelyubina
Russ. Chem. Rev., 2021, **90** (10) 1330 – 1358

https://doi.org/10.1070/RCR5002

Modern physical methods for the molecular design of single-molecule magnets

Valentin V. Novikov, Yulia V. Nelyubina

A.N.Nesmeyanov Institute of Organoelement Compounds, Russian Academy of Sciences, ul. Vavilova 28, 119991 Moscow, Russian Federation

Many paramagnetic metal complexes have emerged as unique magnetic materials (single-molecule magnets), which behave as conventional magnets at the single-molecule level, thereby making it possible to use them in modern devices for data storage and processing. The rational design of these complexes, however, requires a deep understanding of the physical laws behind a single-molecule magnet behaviour, the mechanisms of magnetic relaxation that determines the magnetic properties and the relationship of these properties with the structure of single-molecule magnets. This review focuses on the physical methods providing such understanding, including different versions and various combinations of magnetometry, electron paramagnetic and nuclear magnetic resonance spectroscopy, optical spectroscopy and X-ray diffraction. Many of these methods are traditionally used to determine the composition and structure of new chemical compounds. However, they are rarely applied to study molecular magnetism.
The bibliography includes 224 references.

Contents

1. Introduction 1330
2. Physical basis of single-molecule magnetism 1331
3. Mechanisms of magnetic relaxation in single-molecule magnets 1333
4. Physical methods of investigation of single-molecule magnets 1338
   4.1. Magnetometry 1338
   4.2. Electron paramagnetic resonance spectroscopy 1341
   4.3. Optical spectroscopy 1346
   4.4. Nuclear magnetic resonance spectroscopy 1348
   4.5. X-Ray diffraction 1351
5. Conclusion 1353
6. List of acronyms and designations 1353

1. Introduction

Molecular magnetism is a rapidly expanding interdisciplinary field of research aimed at preparing and investigating molecular materials that have particular magnetic properties.[1,2] Any substance can interact with the magnetic field, but only compounds, the magnetic properties of which are determined by the presence of unpaired electrons, are traditionally assigned to molecular magnets. The classification of molecular magnets according to the type of their interaction with the magnetic field (*e.g.*, ferromagnets, antiferromagnets, ferrimagnets, superparamagnets, spin glasses, *etc.*) is so extensive and the number of publications on this issue is so large that it is impossible to comprehensively address the advances in this field in one review. This review focuses on single-molecule magnets (SMMs)[3] as molecular magnetic materials that have attracted the most attention in recent years and methods of their investigation by modern physical methods used to identify new chemical compounds.

A single-molecule magnet is a compound exhibiting properties of a conventional magnet on the molecular scale.[4] In the general case, the terms 'single-molecule magnets' and 'molecular magnets' are not interchangeable, because molecular magnets traditionally include compounds, the properties of which are determined by other magnetic phenomena,[5] such as the spin transition,[6] magnetic exchange,[7] spin frustration,[8] *etc.*, or by interactions between molecules in one,[9] two[10] or three[11] dimensions. Separate groups include inorganic solid-state,[12] polymeric[13] and hybrid[14] magnetic materials. The discussion of these materials is beyond the scope of our review that intended to focus on coordination and organometallic compounds behaving as single-molecule magnets.

It has long been considered that an individual molecule cannot exhibit macroscopic magnetic properties because conventional ferromagnetism is a cooperative property and, consequently, it can be observed in large particle assemblies. However, back in 1993 Sessoli *et al.*[3] synthesized polynuclear manganese complexes, which are characterized by very slow relaxation of the magnetization, *i.e.*, have superparamagnetic behaviour. Subsequent extensive studies of various paramagnetic compounds[4] revealed SMM properties not only in polynuclear first-row transition metal complexes but also in complexes with a single metal ion,[15] which are sometimes called single-ion magnets. Single-molecule magnets have attracted great worldwide atten-

V.V.Novikov. Doctor of Chemical Sciences, Deputy Director of the INEOS RAS.
E-mail: novikov84@ineos.ac.ru
Y.V.Nelyubina. Doctor of Chemical Sciences, Head of the Laboratory at the same Institute.
E-mail: unelya@ineos.ac.ru
Current research interests: molecular design, physical methods for investigation of the structure of matter, molecular magnetism, crystal chemistry, nature of chemical bonding.

Translation: T.N.Safonova

Received 25 August 2020

© 2021 Uspekhi Khimii, ZIOC RAS, Russian Academy of Sciences and IOP Publishing Limited

tion due to their unique properties and fascinating prospects of their potential use in ultrahigh-density data storage and ultrafast data processing devices and as logic units future quantum computers,[16] the creation of which will lead to the revolution in computing technologies.

Despite the progress achieved in the past three decades in the area of single-molecule magnetism,[17–21] including SMMs that function at liquid nitrogen temperatures,[22] only a small proportion of the available metal complexes were tested as potential SMMs. This is in part due to the low accessibility of the main methods for the identification of SMMs, such as alternating field magnetometry and high-level quantum chemical calculations, which are necessary tools in almost all (with rare exceptions) modern studies on single-molecule magnetism. The objective of this review is to fill this gap. The review may serve as a useful reference for synthetic chemists interested in unique or well-known classes of compounds, which can potentially behave as SMMs, and for specialists in the field of physical methods of investigation of different compounds wanting to expand the scope of their application. The focus is on methods available in chemical institutions † and their application to investigate true SMMs, *i.e.*, molecular compounds that exhibit slow magnetic relaxation in the absence of the external magnetic field.[3]

2. Physical basis of single-molecule magnetism

The distinguishing feature of ferromagnetic materials is the ability to maintain the magnetization acquired from long exposure to a magnetic field, which is associated with the existence of individual domains, where all magnetic moments are aligned in the same direction. The externally applied magnetic field causes a sharp change of the domain boundaries and changes in the magnetization direction within the domain, which is evidently accompanied by the appearance of the hysteresis in the plot of magnetization of the sample *versus* the applied magnetic field. In the absence of a rather strong external magnetic field, the sizes of the domains and the directions of their magnetization remain unchanged and, consequently, magnetized ferromagnetic materials retain magnetization for an almost unlimited time. Due to this distinguishing feature, ferromagnetic materials can be used in data storage devices, such as computer hard discs. However, the minimum individual area of magnetization in such materials, which can store a single bit of data, comprises millions of atoms. This significantly limits the data recording density and, correspondingly, the size of an electronic storage device.

Single-molecule magnets capable of retaining magnetization of individual molecules over long periods of time are free of this drawback. When exposed to an external magnetic field, the unpaired electron spins in such molecules are aligned parallel to the field, and the switching off of this field does not lead to the complete magnetization relaxation, *i.e.*, to the return to a random distribution of spin orientations in the sample, as opposed to other paramagnetic compounds. This is due to the presence of an energy barrier between two opposite orientations of the magnetic moment (bistability) of SMMs, resulting in that the data recorded in the magnetic state of this molecule do not disappear or disappear very slowly (slow magnetic relaxation) after switching off the external magnetic field. The presence of this barrier is associated with the magnetic anisotropy defined as the dependence of magnetic properties on a preferred crystallographic direction.

It is most convenient to consider the factors responsible for the appearance of magnetic anisotropy in SMMs using complexes with 3d transition metal ions. When molecules with unpaired electrons are exposed to a magnetic field, the electronic energy levels of the molecule are split into different levels due to the Zeeman effect. For complexes with a total spin S, this leads to the appearance of $2S + 1$ possible states, each state having its own spin quantum number M_s, which is the sum of the spin quantum numbers m_s of the unpaired electrons in the molecule. In compounds with one unpaired electron or for high-symmetry systems with a large spin S in the absence of the applied magnetic field, all states are energetically degenerate (Fig. 1 *a*,*b*). However, the zero-field splitting that occurs in some cases leads to the partial removal of degeneracy. Depending on the sign of the zero-field splitting energy (D), there are two radically different splitting patterns of magnetic levels. At positive energies D (Fig. 1 *c*), the states $M_s = 1/2$ and $-1/2$ correspond to the ground state (for complexes with a half-integer total spin), thereby allowing, for example, the detection of transitions between these sublevels by electron paramagnetic resonance (EPR) spectroscopy. At negative energies D, the ground state has the maximum $|M_s|$ value for this system (Fig. 1 *d*). In the general case, these transitions are forbidden by selection rules, which allow only transitions accompanied by changes in the M_s value by unity.

If the total spin S is rather large and D has a negative value large in magnitude, the magnetization of the sample in an external magnetic field at a rather low temperature leads to the population only of the state with the minimum value of $M_s = -S$ (Fig. 2). Despite the fact that after switching

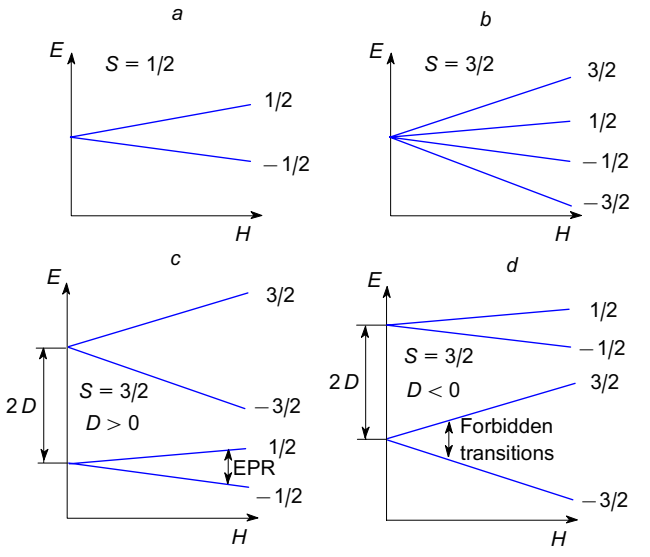


Figure 1. Zeeman splitting of energy levels under applied magnetic field for systems with different total electron spins: *a*, *b*, in the absence of splitting; *c*, *d*, in the presence of magnetic anisotropy. E is the total energy of the system, the fractional numbers are M_s values.

† For this reason, such methods as inelastic neutron scattering,[23] X-ray magnetic circular dichroism spectroscopy,[24] muon spin resonance [25] and high-level quantum chemical calculations are beyond the scope of this review; the advantages and drawback of these methods are considered in detail in the review.[26]

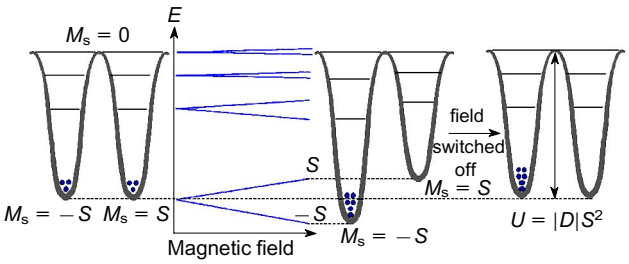


Figure 2. Schematic view of the energy level splitting in SMMs. From the left to right side: at a low temperature, only states with $M_s = \pm S$ are populated; the switching of the external magnetic field causes the level splitting, with the result that only the state with $M_s = -S$ is populated; after the external magnetic field is switched off, the ground state is again doubly degenerate in energy, but the restoration of the equilibrium in the absence of the quantum tunneling of magnetization‡ can be achieved only by overcoming the energy barrier $U = |D|S^2$.

off the magnetic field, the levels with $M_s = \pm S$ become degenerate, these populations cannot be equalized because of the forbiddance of a multiple quantum transition between these two states (except for the cases described below, in which quantum tunneling of magnetization (QTM) is observed). The restoration of the equilibrium in this system, which is a true SMM, can occur through successive single quantum transitions between the states $-S$ and $-S+1$, $-S+1$, $-S+2$, *etc*. This mechanism of magnetic relaxation, called the Orbach mechanism, is related to the overcoming of the energy barrier, which depends on the total electron spin of the system and the zero-field splitting energy: $U = DS^2$ or $U = D(S^2-1/4)$ for half-integer spins.

Hence, compounds with large spins S or with negative D values very large in magnitude can be used to increase the time of demagnetization of SMMs. The latter, in particular, defines the time during which the magnetization is retained in individual elements of the data storage device.

In polynuclear transition metal complexes, individual ions can be coupled in a ferromagnetic mode (as a consequence, the total spin of the compound is equal to the sum of the spins of the individual ions) or an antiferromagnetic mode, which is undesirable because it leads to a decrease in the total spin of the system. Taking into account the quadratic dependence of the barrier to magnetization reversal U on the total spin S, researchers interested in the molecular magnetism have long focused their attention exclusively on the preparation of polynuclear metal complexes with the maximum total spin. The first example of these compounds, exhibiting slow magnetic relaxation in the absence of an applied magnetic field (a distinguishing feature of this SMM), is the mixed-valence manganese complex $[Mn_8^{III}Mn_4^{IV}O_{12}(MeCOO)_{16}(H_2O)_4]\cdot 2\,MeCOOH\cdot 4\,H_2O$ (Fig. 3), often denoted as Mn_{12} (see Ref. 27) with the total spin $S = 10$, the zero-field splitting energy $D = -0.46\ cm^{-1}$ and the barrier to magnetization reversal $U = 46\ cm^{-1}$. In this case, a relatively small increase in the total spin to 12 in the complex with six manganese ions[28] leads to an increase in U to $62\ cm^{-1}$ despite the observed decrease in the magnetic anisotropy D to $-0.43\ cm^{-1}$.

‡ The quantum tunneling of magnetization (QTM) traditionally means a phenomenon in which a particle penetrates a barrier of potential energy with a height greater than the total energy of this particle without the energy loss, *i.e.*, the possibility of the particle passing through a region, which cannot be penetrated in the classical world.

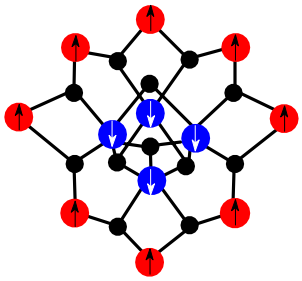


Figure 3. Structure of the Mn_{12} complex with manganese(IV) ($S = 3/2$) and manganese(III) ($S = 2$) ions coloured in red and blue, respectively. The orientations of electron spins localized on the Mn^{III} and Mn^{IV} ions are indicated by arrows. The Figure was prepared by the authors using the data of Ref. 3.

The progress in coordination chemistry has provided routes to the synthesis of polynuclear complexes with much larger total spins, *e.g.*, complexes with forty two iron ions ($S = 45$)[29] or with nineteen manganese ions ($S = 83/2$).[30] Nevertheless, these complexes cannot be assigned to SMMs because they do not have magnetic anisotropy ($D = 0$) due to several factors.

First, in order for a molecule to behave as a single-molecule magnet, not only the number of ferromagnetically coupled ions in one molecule should be increased, which provides the maximum possible total spin, but also the magnetic anisotropy should be retained, which requires that the directions of anisotropy axes of individual ions should be aligned with each other or at least these axes should not be oppositely directed. For example, in the record compound with the total spin $S = 45$,[29] the anisotropies of individual metal ions are mutually compensated, resulting in the isotropic ground state of this complex.

Second, the zero-field splitting energy also depends on the total spin of the system in an inverse quadratic manner.[31] Therefore, the final value of the barrier to magnetization reversal is determined not only by the total spin but also by the D value.[32] Besides, the zero-field splitting energy is very sensitive to slight changes in the electronic structure, which significantly complicates the search for the principles of molecular design of new SMMs.

In all these cases, the key concept is the presence of the orbital momentum L in SMMs in the presence of energetically degenerate and partially filled (but not half-filled) orbitals. For first-row transition metal ions, the ligand field effect generally causes the splitting of orbitals, resulting in that the orbital momentum is equal or close to zero. Slight deviations, observed in many cases, are due to the fact that the spin–orbit coupling brings about the mixing of the ground and excited electronic states giving rise to the zero-field splitting. However, complexes of lanthanides and (in rare cases)[33] first-row transition metals can retain the orbital momentum, resulting in very high magnetic anisotropy. The f orbitals of lanthanide atoms are localized, their energies depend only slightly on the coordination environment, and the non-quenched orbital momentum L interacts with the total spin momentum S giving rise to the total angular momentum J; $|L-S| \leqslant J \leqslant |L+S|$.

In these case, it has often been said that S is not a good quantum number. This means that not only the spin magnetic moment but also the total angular momentum J are required to describe the magnetic properties of the molecule. Generally, for lanthanides complexes, the large value of J for the ground state multiplet is an important, although not sufficient, requirement for the appearance of a

high magnetic anisotropy and, as a consequence, for the manifestation of the SMM properties.

The patterns of energy levels, similar to those shown in Fig. 1, provide insight into the factors responsible for the appearance of magnetic anisotropy in some metal complexes. However, a more formal approach is required for the detailed analysis. Single-molecule magnets are usually described in terms of the spin-Hamiltonian formalism.[34] The spin-Hamiltonian is an operator obtained by the averaging of the full Hamiltonian of the system $\widehat{H}_{\rm f}$, which describes its ground state in the stationary Schrödinger equations, over all non-spin coordinates. The equation with the Hamiltonian $\widehat{H}_{\rm f}$ can be solved, *i.e.*, its eigenvalues and eigenfunctions can be determined, only in an approximate way. The complexity of even this approximate solution rapidly increases with increasing size of the system. However, the magnetic properties of the system are usually determined solely by interactions of unpaired electrons with each other and with magnetically active nuclei. Since the corresponding contribution to the total energy of the system is several tens of Joules per mole in magnetic fields of a few Tesla, the magnetic field-induced change in its value is very small

$$E = E_0 + \sum_n \frac{\partial E}{\partial s_n} s_n + \frac{1}{2}\sum_{n,k} \frac{\partial^2 E}{\partial s_n \partial s_k} s_n s_k \qquad (1)$$

where E_0 is the contribution to the total energy of the molecule independent of the spin coordinates s_n. The operator describing the spin-dependent term of equation (1) is called the spin-Hamiltonian. For example, the popular spin-Hamiltonian corresponding to the pattern of energy levels in Fig. 1 takes the following form:

$$\widehat{H} = D\left[\widehat{S}_z^2 - \frac{S(S+1)}{3}\right] + \mu_{\rm B} B g \widehat{S} \qquad (2)$$

Here D is the axial component of the zero-field splitting energy, g is the electronic g-tensor, $\mu_{\rm B}$ is the Bohr magneton and B is the magnetic induction.

As opposed to the full Hamiltonian, the search for the eigenvalues of the operator similar to the spin-Hamiltonian (2) is a rather trivial problem, the solution of which allows the description of a number of properties of the system, including those determined by magnetometry or spectroscopy. For example, for the barrier to magnetization reversal in SMMs with integer or half-integer total spins S, this leads, respectively, to the following equations:

$$U = E_{M_S^{\max}} - E_{M_S^{\min}} = \qquad (3)$$
$$= D\left[S^2 - \frac{S(S+1)}{3}\right] + D\frac{S(S+1)}{3} = DS^2$$

$$U = E_{M_S^{\max}} - E_{M_S^{\min}} = \qquad (4)$$
$$= D\left[S^2 - \frac{S(S+1)}{3}\right] - D\left[\frac{1}{4} - \frac{S(S+1)}{3}\right] = D\left(S^2 - \frac{1}{4}\right)$$

The spin-Hamiltonian (2) is suitable for the description of systems with an almost completely quenched orbital momentum, including most of first-row transition metal complexes. However, this spin-Hamiltonian cannot be applied to complexes, in which the orbital momentum makes a significant contribution to the magnetic properties. This is particularly the case with lanthanide compounds. For the description of such complexes, the spin – orbit coupling should be explicitly taken into account. In this case, the following Hamiltonian is commonly employed:

$$\widehat{H} = \sum_{k=2,4,6} \sum_{q=-k}^{+k} B_k^q \widehat{O}_k^q \qquad (5)$$

where $\widehat{O}_k^q$ are polynomial functions of the total momentum operators, so-called Stevens operators tabulated in the monograph,[35] B_k^q are the corresponding coefficients. The Hamiltonian (5) can include up to 27 parameters. This number is significantly smaller for high-symmetry metal complexes, due to which their magnetic properties can be described using a few coefficients B_k^q.

The condition for the use of the Hamiltonians (2) and (5) is based on the following assumption. Each energy level belongs to the pure state with the only value of the spin or the total angular momentum. However, the spin – orbit coupling often makes it necessary to consider each energy level as a linear combination of the levels with different values of S or J. This greatly complicates the description of SMMs and requires the use of a wide combination of modern physicochemical methods to determine the characteristic features of their electronic structures and related magnetic properties.

3. Mechanisms of magnetic relaxation in single-molecule magnets

The magnetic relaxation (spin relaxation or relaxation of the magnetization) is the establishment of a thermodynamic equilibrium between magnetic moments, resulting in the return of the system from the excited non-equilibrium state, arising from magnetic degrees of freedom, to equilibrium. The magnetic relaxation time determines the potential for practical applications of a particular SMM. Generally, magnetic relaxation is a result of several competing physical processes, the relative contributions of which depend on the composition and structure of the compound, its phase state, intermolecular interactions, the temperature and the external magnetic field. Single-molecule magnets are characterized by a large barrier to magnetization reversal. However, in many cases it is insufficient for the retention of magnetization of the molecules over a long period of time due to the existence of alternative mechanisms of relaxation, which are not related to the overcoming the energy barrier U. Hence, the investigation of these processes and the influence of the chemical structure of SMMs on their relative efficiency is a challenge in studying SMMs.

An external disturbance, *e.g.*, the applied magnetic field, brings the system from an equilibrium. After switching off this disturbance, the system returns to the equilibrium with the characteristic constant T_1, called the spin-lattice relaxation time. Spin-lattice relaxation processes are caused by the interaction of the spin system with its environment, *i.e.*, the crystal lattice. These processes can occur in the absence of the crystal lattice (*e.g.*, in solutions). However, in the latter cases, these processes are usually related to other mechanisms.

The spin-lattice relaxation in solids gives rise to spin-phonon coupling between electronic and nuclear spins of the atoms in the molecule and quantized elastic vibrations of the crystal lattice (phonons) accompanied by the emission (absorption) of the energy quantum by the spin system and its absorption (emission) by the crystal lattice. This

transition between two levels of the spin system can occur in the presence of an oscillating electromagnetic field, which is indicative of mechanisms giving rise to the corresponding field through crystal lattice vibrations. According to one of these mechanisms,[36] it is assumed that the displacement of adjacent magnetic ions in the crystal lattice in the course of vibrations causes changes in the local magnetic field and, correspondingly, the transition between the energy levels of the system. Hence, the spin–spin nature of magnetic relaxation is postulated. However, in this case,[37] the efficiency of the so-called direct relaxation process, which involves the emission of one energy quantum that is absorbed by the crystal lattice as one phonon (Fig. 4 *a*), is very low because of a low phonon density at the resonance frequency of the spin system. As a result, the expected magnetic relaxation times were overestimated from the experimental data by several orders of magnitude. Besides, if the magnetic relaxation would be caused by interactions between adjacent paramagnetic ions in the crystal lattice, the cocrystallization of a paramagnetic compound with an excess of an isostructural diamagnetic analogue (*i.e.*, in the case of diamagnetic dilution), the magnetic relaxation time would be drastically increased with decreasing concentration of the corresponding ions; however, the latter was not observed.

According to another description of the spin–phonon coupling, which was proposed by Heitler and Teller [39] and then was developed in detail by Van Vleck,[40] the crystal lattice vibrations give rise to a fluctuating electric field due to crystal field changes upon varying the ion–ligand distance. This approach provides the correct prediction of magnetic relaxation times for a number of transition metal salts [40] at nearly liquid helium temperatures. However, at higher temperatures, the measured values were much smaller than the predicted magnetic relaxation times due to an insignificant energy difference between the corresponding magnetic levels and a low phonon density with this energy.

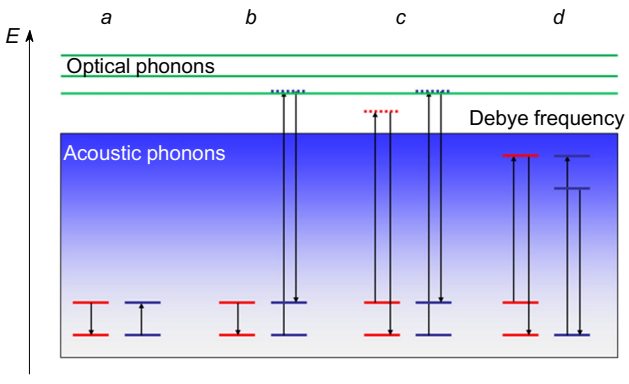


Figure 4. Schematic view of the main mechanisms of magnetization spin-lattice relaxation processes in SMMs:[38] *a*, the direct process; *b*, the first-order Raman process; *c*, the second-order Raman process; *d*, the Orbach process. The red horizontal lines represent the energy levels of the spin system; the blue lines, the energy levels of the lattice; the dashed lines, the virtual state frequencies higher than the Debye frequency. The blue gradient indicates an increase in the density of high-energy acoustic phonons and their disappearance at frequencies higher than the Debye frequency. The discrete levels corresponding to optical phonons are highlighted with green lines. Reproduced with the permission of Royal Society of Chemistry.

The two-phonon Raman and Orbach mechanisms are alternative to the one-phonon direct relaxation mechanism. In many cases, two-quantum processes can be ignored; however, the phonon absorption and the simultaneous phonon emission at another frequency play an important role in magnetic relaxation. For example, the existence of vibrations with frequencies ω_1 and ω_2 in the crystals means that their summation can give rise to vibrations with frequencies $(\omega_1 \pm \omega_2)$.

Since each pair of phonons with an appropriate energy difference can cause a transition with the frequency $(\omega_1 - \omega_2)$, taking into account the phonon spectral energy density (Fig. 5), this two-quantum relaxation process (called the Raman process by analogy with the Raman scattering effect in optical spectroscopy) is much more efficient than the direct process at high temperatures. It is also important that the transition frequencies ω_1 and ω_2 may correspond to the virtual states lying outside the phonon spectrum. Depending on whether the energy exchange involves only the virtual states of the crystal lattice (Fig. 4 *b*) or it occurs between the virtual states of the lattice and the spin system (Fig. 4 *c*), there are first- and second-order Raman processes.

Another two-quantum process, which should be taken into account in the design of SMMs, makes an important contribution to the magnetic relaxation of the spin system if the latter has low-lying excited states. This process, named after Orbach, involves the phonon absorption by the spin system, resulting in the transition of the latter to the excited state, and the subsequent emission of a higher-frequency phonon accompanied by the return of the system to the ground state (Fig. 4 *d*). Since the spin-phonon Hamiltonian contains terms of second order with respect to the spin operators, the spin–phonon coupling can lead to transitions of SMM from the state $|M_s\rangle$ to the states $|M_s \pm 1\rangle$ and (with a much lower probability) $|M_s \pm 2\rangle$. For example, the interaction with lattice vibrations in the Mn_{12} complex with the spin $S = 10$ can lead to absorption of one quantum corresponding to the energy difference between the states with $M_s = -10$ and $M_s = -9$ and the transition between these two states. The absorption of additional phonons allows transitions between the levels $M_s = -8, -7$, *etc.* up to the state with $M_s = 0$ lying at the top of the energy barrier. The further evolution of the system may involve the phonon emission, *i.e.*, the excitation of crystal lattice vibrations, which finally will result in the return of the

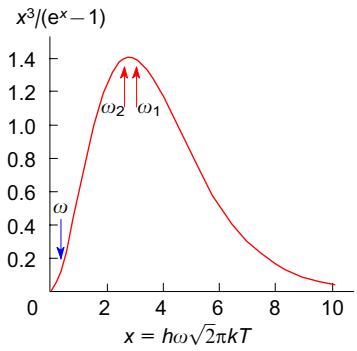


Figure 5. Plot of the phonon spectral energy density. The blue arrow indicates the density of phonons responsible for the direct relaxation mechanism (ω is the magnetic transition frequency in the system), the red arrows correspond to one set of vibrations giving rise to two-quantum relaxation processes between the spin levels with $\Delta E = h\omega = h(\omega_1 - \omega_2)$. The Figure was prepared by the authors using the data of Ref. 37.

system to the initial state with $M_s = -10$ or to the state with $M_s = +10$. The probability of the transition between the states with $M_s = -10$ and $M_s = 0$ is determined by the product of the probabilities of individual transitions, and the expression for the magnetic relaxation time (τ) takes the following form:

$$\tau = \tau_0 \exp\left(\frac{\Delta E}{kT}\right) \quad (6)$$

where $\Delta E = E(0) - E(10)$ is the energy difference between the states with $M_s = -10$ and $M_s = 0$, and the factor τ_0 depends, in particular, on elements of the spin-phonon Hamiltonian. According to this mechanism, the magnetic relaxation time has an Arrhenius temperature dependence, which is often used to determine the barrier to magnetization reversal U in the absence of other mechanisms.

The so-called phonon bottleneck effect need to be mentioned. The above-described relaxation mechanisms imply a much higher heat capacity of phonons compared to that of spins. Hence, the energy, which leaves the spin system *via* magnetic relaxation, is absorbed by the corresponding phonons and is immediately distributed in the crystal lattice, without changing its temperature, and is then transferred to an external thermostat with an infinite heat capacity. This approximation is usually valid; however, the phonon bottleneck effect may occur in some cases. For example, if the energy transfer time between resonance and non-resonance phonons or the energy transfer time from the latter to the thermostat is longer than the spin – phonon relaxation time, the spin dynamics of the system, manifested as a slow magnetic relaxation and the presence of magnetic hysteresis, may be not related to the SMM properties but can be caused by crystal packing effects.

Another important mechanism of magnetic relaxation in SMMs is based on the quantum tunneling of magnetization. Generally, SMMs do not display this effect in the absence of the applied magnetic field, when the sublevels on both sides of the energy barrier are energetically degenerate (Fig. 6, position *1*). In the case of mixing of wave functions with the opposite sign of the spin quantum number M_s, the transition between these sublevels has a non-zero probability and, as a consequence, it can make a significant contribution to magnetic relaxation, which is actually observed at rather low temperatures (< 10 K).

In systems, the magnetic properties of which are described by the spin-Hamiltonian (2), only states $M_s = \pm S$ states are populated at low temperatures.

The states $M_s = +S$ and $M_s = -S$ are orthogonal to each other, their wave functions do not mix and, consequently, the tunneling is impossible. However, the wave functions can mix due to a perturbation caused, for example, by the transition from the axial to rhombic symmetry of the system,

$$\hat{H}_{rh} = E(\hat{S}_x^2 - \hat{S}_y^2) \quad (7)$$

Since the spin-Hamiltonians (7) and (2) do not commutate with each other, the states of the spin-Hamiltonian

$$\hat{H} = \hat{H}_0 + \hat{H}_{rh} \quad (8)$$

contain mixed eigenfunctions, including those with different signs of M_s, thereby allowing the quantum tunneling of magnetization. The probability of this process is usually low particularly for systems with a large total spin S, for which this probability is non-zero only in terms of the high-order perturbation theory. Besides, for Kramers ions with a half-integer spin S, the rhombicity of the zero-field splitting tensor is insufficient for the appearance of quantum tunneling of magnetization according to the Kramers theorem.[41] However, the mixing of eigenfunctions of the Hamiltonian (2) can also be caused by hyperfine interactions with magnetically active nuclei or by external magnetic fields produced, for example, by other paramagnetic centers in the molecule.

Besides, the quantum tunneling of magnetization can occur between degenerate excited states (see Fig. 6, position *2*), including higher-order excited states (see Fig. 6, position *3*). This process, referred to as thermally activated tunneling, is one of the main magnetic relaxation pathways at relatively high temperatures. The overlap of the wave functions of states on both sides of the potential barrier increases with approaching the top of the barrier, thereby increasing the probability of QTM. Meanwhile, the probability of absorption of phonons with the corresponding energy exponentially decreases for higher-order excited states. Hence, the thermally activated tunneling *via* different excited states[42] or the relaxation through several mechanisms[43] are possible for the same molecular system depending on the chosen temperature. This leads to a substantial decrease in the effective barrier to magnetization reversal U_{eff}; in some cases, to the absence of SMM properties even at very low temperatures due to QTM between sublevels of the ground state.

The contribution of QTM to the magnetic relaxation in SMMs is generally reduced by applying the external magnetic field to remove the degeneracy of the corresponding states (see Fig. 2). However, a rather strong field can, on the contrary, cause the energy degeneracy of the levels corresponding to the states $+M_s$ and $-M_s + n$ (see Fig. 6, position *4*), because the energy of levels with positive M_s increases, while the energy of levels with negative M_s decreases due to the Zeeman effect. In this case, QTM significantly contributes to the magnetic relaxation in SMMs (Fig. 7), which appears as characteristic steps in the plot of the magnetization of the sample *versus* the applied field. For example, the efficient QTM is responsible for a non-monotonic dependence of the magnetic relaxation time on the applied magnetic field for Mn_{12},[44] with the fast magnetization reversal at some magnetic field strengths,[45] and the appearances of steps in the magnetic hysteresis loop (Fig. 8). The horizontal regions of the hysteresis loop correspond to the values of the applied magnetic field, at which the levels of the states with $+M_s$ and $-M_s + n$, are

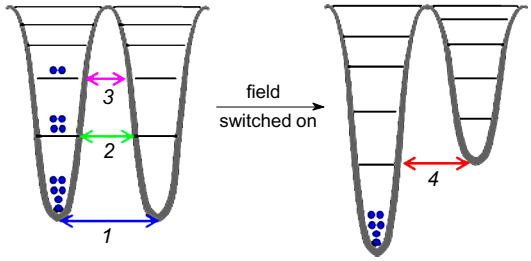


Figure 6. Schematic view of QTM through the ground state (*1*), QTMs thermally activated *via* the first (*2*) and second (*3*) excited states and QTM caused by the applied magnetic field (*4*).

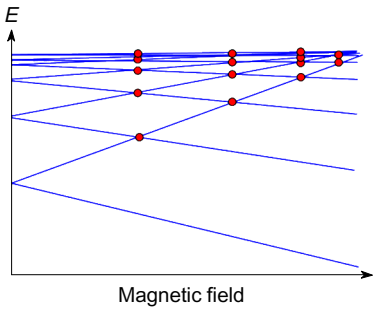


Figure 7. Plot of the energy levels in SMMs with axial magnetic anisotropy *versus* the external magnetic field. The red dots represent the field strengths corresponding to intersections of the levels at which QTM can be observed.

not degenerate and QTM is impossible, resulting in long relaxation times.

The quantum tunneling of magnetization is a very interesting process, which clearly demonstrates the quantum nature of SMMs. However, this process is usually undesirable in practical applications of SMMs for ultra-high-density data storage, because it leads to the fast loss of magnetization even at the lowest temperatures. In order to reduce the contribution of QTM, it is necessary to gain a deep understanding of the factors responsible for this process. For example, in the simplest case, non-Kramers ions can be replaced by Kramers ions because, according to the Kramers theorem, QTM is forbidden in SMMs with an odd number of unpaired electrons.[41] Another way of providing high magnetic anisotropy is to synthesize low-coordinate first-row transition metal complexes [most often, iron(II)][48,49] with a linear geometry,[50] which ensures large zero-field splitting[51] due to the preservation of the orbital momentum[52] that remains unquenched by the crystal field.[53] However, even in the case of a high barrier to Orbach relaxation under an applied magnetic field, these compounds (*e.g.*, $Fe[C(SiMe_3)_3]_2$ with $D = 146\ cm^{-1}$) were found to display fast magnetization relaxation under zero field *via* QTM[54] due to the non-Kramers nature of the iron(II) ion with the high-spin d^6 electronic configuration characterized by the presence of four unpaired electrons. It should be noted that the use of isostructural iron(I) complexes made it possible to reduce the efficiency of QTM due to the appearance of a high barrier to Orbach relaxation under zero field; for example, this barrier for $[K(crypt222)]Fe[C(SiMe_3)_3]_2$ was 226 cm^{-1}, which was at one time the record value for SMMs with first-row transition metal ions.[55] Unfortunately, a change in the number of unpaired electrons usually leads to a change in the molecular geometry of SMMs accompanied by the loss of SMM properties. Therefore, the use of Kramers ions as a source of magnetic anisotropy remains one of the major principles of molecular design of SMMs with first-row transition metals.

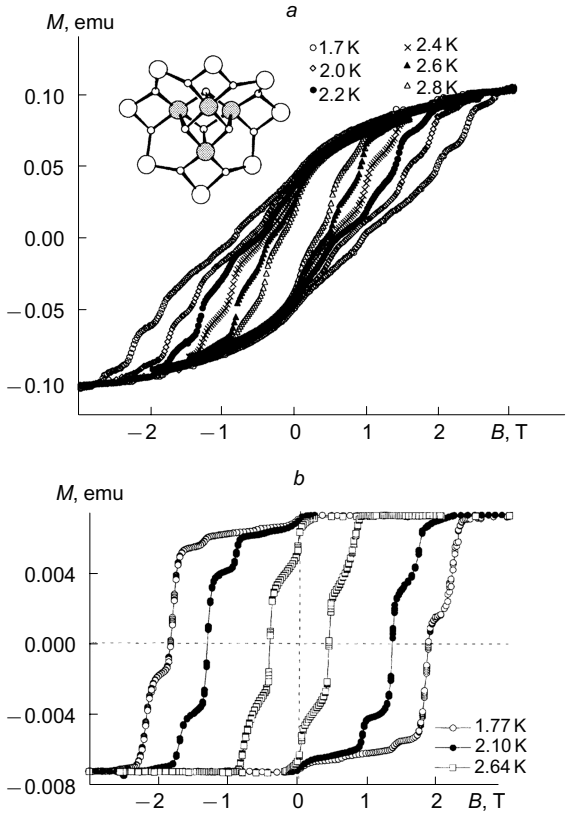


Figure 8. Magnetic hysteresis loops for a finely crystalline sample of Mn_{12} aligned in the magnetic field (*a*)[46] and for single crystals of this SMM (*b*).[47] Reproduced with the permission of American Physical Society.

However, QTM may occur even in SMMs with an odd number of unpaired electrons in the presence of an appropriate perturbation, for example, the rhombicity of the zero-field splitting tensor. For complexes with strictly trigonal or higher-symmetry coordination geometry, the spin-Hamiltonian should have strictly axial symmetry, which does not allow the appearance of QTM. Any deviation from this configuration, including distortions caused by the Jahn–Teller[56] or Renner–Teller effects,[57] gives rise to QTM and the attendant degradation of magnetization.[58] Correspondingly, another principle of molecular design of SMMs is the retention of the highest-symmetry coordination environment of the metal ion, for example, using a rigid multudentant ligand.

Finally, the contribution of QTM can be reduced using an approach based on the exchange bias effect associated with the internally applied magnetic field.[59,60] For example, the complex $Mn_4O_3Cl_4(O_2CEt)_3(py)_3$ (Mn_4, $S = 9/2$)[61] forms the dimer $[Mn_4]_2$, in which two C_3-symmetric monomers are aligned along the crystallographic axis S_6 (Fig. 9 *a*). Due to this dimerization, the magnetic hysteresis loop (Fig. 9 *c*) did not show a sharp jump of magnetization at zero magnetic field, which was observed in the starting Mn_4 complex (Fig. 9 *b*). Therefore, $[Mn_4]_2$ was the first SMM, in which no sharp increase in the probability of QTM at zero field was observed.[59]

The developed approach to decrease the contribution of QTM to the magnetic relaxation in SMMs with transition metal ions *via* exchange interactions was successfully applied to design SMMs based on lanthanide compounds, including triple- (see Ref. 62) and quadruple-decker[63] phthalocyanine complexes. For example, the covalent binding of two terbium double-decker phthalocyanine complexes (Fig. 10) led to a significant decrease in the probability of QTM at zero field *via* dipole–dipole interactions between two paramagnetic terbium ions.

Meanwhile, these interactions can, on the contrary, initiate the activation of QTM similarly to magnetic fields caused by hyperfine interactions between the electron spin and magnetically active nuclei[65] in the molecule or by the presence of other paramagnetic centers in the crystalline

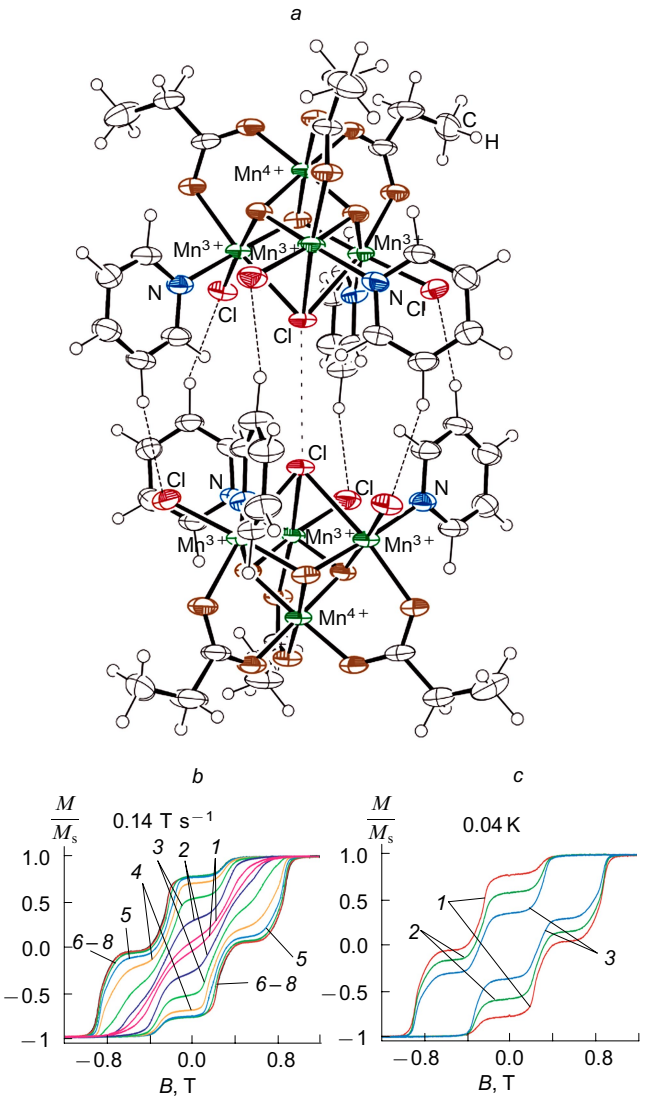


Figure 9. Structure of the dimer $[Mn_4]_2$ (*a*) and the magnetic hysteresis loops for single crystals of the starting manganese complex Mn_4 (*b*) and its dimer $[Mn_4]_2$ (*c*).[59] Reproduced with the permission of Springer Nature.
b: T = 1.0 (*1*), 0.8 (*2*), 0.7 (*3*), 0.6 (*4*), 0.5 (*5*), 0.4 (*6*), 0.3 (*7*), 0.04 K (*8*); *c*: B/t = 0.14 (*1*), 0.017 (*2*), 0.004 T s^{-1} (*3*).

sample.[66] For example, the spin dynamics in magnetically saturated samples is often determined by cooperative effects caused by intermolecular interactions rather than by molecular effects associated with the electronic structure of individual molecules.[67] In some cases, compounds can show magnetic hysteresis at low [68] (or room) [69] temperatures due to magnetic interactions between individual molecules.[70] Therefore, in order to unequivocally confirm the molecular nature of slow magnetic relaxation,[71] it is necessary to prepare a diamagnetically diluted sample [72, 73] by the cocrystallization of SMM with an excess of an appropriate isostructural diamagnetic analogue.[74]

Besides, it is important to evaluate the contributions of different mechanisms of magnetic relaxation (QTM, direct and Raman processes), which hinder the SMM behaviour, to the quantum dynamics of the system. If the quantum dynamics involves several such mechanisms, it is generally described using the magnetic relaxation rate (τ^{-1}), which is an additive value, rather than the magnetic relaxation time (τ). The probability of all these mechanisms of magnetic relaxation depends on the electronic and three-dimensional structure of SMM molecules and on the vibronic structure of their crystals. Until recently, the only route to the quantitative interpretation of experimental data on the magnetic relaxation in SMMs was based on phenomenological equations proposed for simple models.[37]

In the case of a direct process for ions with an odd number of unpaired electrons,[37] the magnetization relaxation rate depends on the magnetic field strength and the temperature

$$\tau^{-1} \approx H^3 \operatorname{cth} \frac{g\mu_B H}{2kT} \tag{9}$$

On the condition that $g\mu_B H/2kT \ll 1$

$$\tau^{-1} = AH^2T \tag{10}$$

where A is the phenomenological constant, which depends, for example, on the potential of the electric field caused by

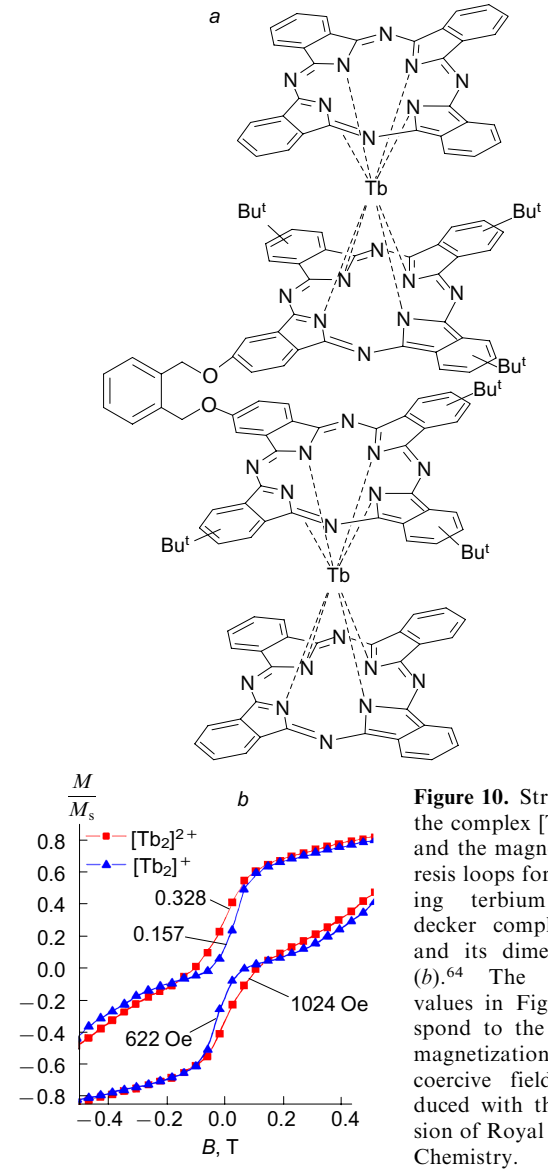


Figure 10. Structure of the complex $[Tb_2]^{2+}$ (*a*) and the magnetic hysteresis loops for the starting terbium double-decker complex $[Tb]^+$ and its dimer $[Tb_2]^{2+}$ (*b*).[64] The numerical values in Fig. *b* correspond to the remanent magnetization and the coercive field. Reproduced with the permission of Royal Society of Chemistry.

crystal lattice deformations. For Kramers ions,[75] the corresponding equations take the form

$$\tau^{-1} \approx H^5 \operatorname{cth} \frac{g\mu_B H}{2kT} \tag{11}$$

$$\tau^{-1} = AH^4T \tag{12}$$

In the presence of hyperfine interactions, the direct relaxation process for Kramers ions should also be described [38] using equation (10) rather than (12).

Since the contribution of QTM to the relaxation of the system at rather low temperatures is temperature-independent, the tunneling rate for two states with m_s and $-m_s$, which differ in energy by $\Delta E = \hbar\omega_T$ and have the lifetime τ_m, is [76]

$$\tau^{-1} = \frac{4\omega_T^2\tau_m}{1+\tau_m^2(E_S - E_{-S})^2/\hbar^2} \tag{13}$$

where the difference $E_S - E_{-S}$ provides the dependence of the efficiency of QTM on the external magnetic field.[77] The replacement of unknowns by the phenomenological constants B_1 and B_2 leads to a simple equation for the QTM rate

$$\tau^{-1} = \frac{B_1}{1+B_2H^2} \tag{14}$$

Finally, the temperature dependence of the probability of the two-quantum Raman process is described by the following power function:

$$\tau^{-1} = CT^n \tag{15}$$

where C is the phenomenological constant related to the vibronic structure of the SMM, and the exponent n depends mainly on the nature of the paramagnetic ion. In the simplest case of Kramers and non-Kramers ions,[37] n is 9 and 5, respectively. However, in the presence of low-lying excited states [78] or taking into account optical phonons,[79] n can vary from 2 to 12.[80]

A combination of equations (9)–(15) with (6) for the Orbach process leads to the following equation:

$$\tau^{-1} = AH^mT + \frac{B_1}{1+B_2H^2} + CT^n + \tau_0^{-1}\exp\left(\frac{-U}{kT}\right) \tag{16}$$

A plenty of variables in equation (16), the values of which cannot be estimated directly from the experimental data, is indicative of a significant overparameterization of this equation, *i.e.*, of the absence of a single set of parameters, which can be used to fit the temperature or field dependence of the relaxation time in SMMs. These variables include the Orbach barrier to relaxation U as a very important parameter for SMMs. Hence, the analysis of these data should be performed with great caution. For example, the analysis of the data at a temperature of 4 K or lower usually allows the mitigation of the effects of two-quantum Orbach and Raman processes. This makes it possible to separate the contributions of QTM and the direct relaxation mechanism based on their different temperature and magnetic field dependences, while the application of an external magnetic field allows the elimination of the contribution of QTM at all temperatures. The resulting values of A, B_1, B_2 and m are then employed to determine other parameters by the combined analysis of all experimental data, including the plots of magnetic relaxation times *versus* the temperature and the external magnetic field. Since even this approach does not necessarily provide the only solution of this optimization problem, any additional data on SMM, in particular, on its electronic structure, can reduce the number of unknowns in equation (16).

4. Physical methods of investigation of single-molecule magnets

Virtually all physical methods suitable for the characterization of chemical compounds can be applied to study SMMs. However, this review focuses on methods, which can be used to observe slow magnetization relaxation (which is usually done by magnetometry and less commonly by magnetic circular dichroism spectroscopy) and also to determine the characteristic features of the electronic structures of the ground and excited states that give rise to SMM properties. Methods, which have a limited applicability (*e.g.*, Mössbauer spectroscopy [81] or polarized neutron diffraction [82]) or which require expensive and difficult-to-access equipment (*e.g.*, X-ray magnetic circular dichroism,[83–85] muon spin spectroscopy [86–88] and inelastic neutron scattering spectroscopy [23, 89, 90]), are also beyond the scope of this review. An interested reader is advised to read dedicated reviews (see, for example, the reviews [91, 92]).

4.1. Magnetometry

Conventional magnetometry experiments involve direct magnetization measurements of a sample, which is moved in a magnetic field between two induction coils, which differ in the winding direction (a first-order gradiometer). According to Faraday s law, changes in the magnetic flux through the circuit produce a current, the EMF of which is proportional to the rate of the change of magnetic flux. The application of gradiometers makes it possible to eliminate the effect of the external magnetic field, so that the measured voltage is determined only by the magnetization of the sample under study.

The induced current can be directly measured with a phase-sensitive detector based on a synchronous amplifier incorporated in a vibrating-sample magnetometer.§ A higher sensitivity of measurements can be provided through inductance between the gradiometer and superconducting quantum interference devices. Experiments are performed using both superconducting quantum interference devices and vibrating-sample magnetometers. The former are characterized by much higher sensitivity, while the latter can be employed to perform measurements in a wider range of external conditions, for example, under higher magnetic fields.

Regardless of the type of the magnetometer, the magnetization of the sample is generally measured at different external magnetic fields and temperatures because of the following reasons. In a simple two-level system with $S = 1/2$ at a fixed temperature under an externally applied magnetic field, the spin levels are split due to the Zeeman effect. At low magnetic fields (the red line in Fig. 11 *a*), the energy difference between the corresponding levels is small, resulting in a small difference in their populations and, conse-

§ This system is sometimes called the Foner magnetometer.[93]

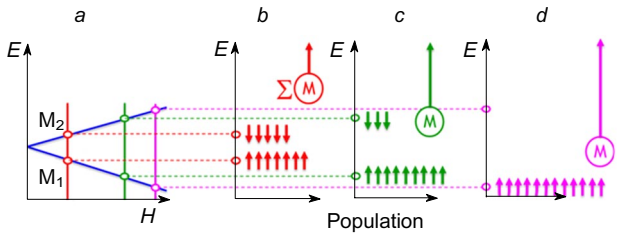


Figure 11. Schematic view of the appearance of the field dependence of magnetization at a fixed temperature. *a*–*d*, see the text. Short arrows indicate the orientations of individual spins; long arrows, the total magnetization.

quently, a small total magnetization (Fig. 11 *b*). An increase in the magnetic field (the green line in Fig. 11 *a*) leads to an increase in the difference in the population of these levels and the enhancement of the total magnetization of the sample (Fig. 11 *c*). Finally, once a particular external magnetic field is achieved, the energy difference between the Zeeman levels becomes much larger than kT and, consequently, the population of the upper component of the doublet at a fixed temperature becomes impossible (Fig. 11 *d*). A further enhancement of the applied magnetic field will not lead to an increase in the total magnetization of the sample (Fig. 12 *a*), *i.e.*, the magnetic saturation will be reached.

However, most experiments are performed in magnetic fields insufficiently strong to cause the magnetic saturation. In these cases, the magnetization of the sample is a linear function of the field; the slope of this plot is called the magnetic susceptibility χ (see Fig. 12 *a*). Since the populations of the corresponding levels depend on the temperature of the sample, its magnetic susceptibility is also temperature-dependent. Generally, this dependence is inverse in character and is given by the Curie law (Fig. 12 *b*). Hence, the magnetometry data are often represented as temperature dependences of the inverse magnetic susceptibility $1/\chi$ (Fig. 12 *c*), χT (Fig. 12 *d*) or the effective magnetic moment μ_{eff} (Fig. 12 *e*). The latter two parameters are used most often because, according to the Curie law, they are temperature-independent

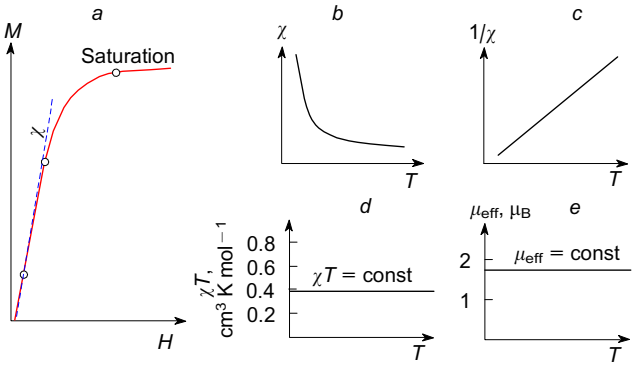


Figure 12. Different representations of the magnetometry data under a direct current magnetic field: the field dependence of magnetization of the sample at a fixed temperature (*a*) and the temperature dependences of the magnetic susceptibility χ (*b*), the inverse magnetic susceptibility (*c*), the χT (*d*) value and the effective magnetic moment μ_{eff} (*e*).

$$\chi T = \frac{N_A g^2 \mu_B^2}{3k} S(S+1) \tag{17}$$

$$\mu_{\text{eff}} = 2.828\sqrt{\chi T} \tag{18}$$

where N_A is Avogadro s number and g is the isotropic g-factor. If the Curie law is obeyed (see below), the χT value or the effective magnetic moment μ_{eff} can be used to estimate the number of unpaired electrons in the system provided that the orbital momentum does not contribute significantly to its magnetic properties.

In the absence of strong spin–orbit coupling,[94] the Curie law is valid for isolated paramagnetic molecules. Therefore, the deviation of χT from the constant value with changes in the temperature are attributed to different kinds of magnetic anomalies, such as the presence of strong magnetic interactions (for example, antiferromagnetic), the spin state transition or high magnetic anisotropy. Hence, the analysis of magnetometry data in a direct current magnetic field is considered as one of the main methods for the approximate evaluation of magnetic anisotropy.

The prospects of the use of a particular compound as SMM can be evaluated based on the analysis of the field dependences of magnetization; the magnetization saturation for highly anisotropic ions often cannot be achieved even in very strong magnetic fields.[95] Another evidence of high magnetic anisotropy is a decrease in χT with decreasing temperature, which, however, can be observed due to the spin transition to the low-spin state or antiferromagnetic interactions. Besides, the χT values, which are much higher than those predicted by equation (17), may be indicative of the significant orbital contribution and, as a consequence, of a large D value. Unfortunately, all these signs are qualitative in nature and cannot serve to unambiguously answer the questions as to whether the compound under consideration exhibits SMM properties and whether it has significant magnetic anisotropy.

An approach based on the quantitative interpretation of magnetometry data in direct current magnetic field is more informative. In this approach, the dependence of magnetization of the sample on the applied magnetic field and the temperature dependence of magnetic susceptibility are modeled simultaneously with an appropriate Hamiltonian, which most often takes the following form:

$$\widehat{H} = D\left[\widehat{S}_z^2 - \frac{S(S+1)}{3}\right] + E(\widehat{S}_x^2 - \widehat{S}_y^2) + \mu_B B g \widehat{S} \tag{19}$$

Here E is the rhombicity of the zero-field splitting tensor, which characterizes the difference in the magnetic susceptibility of the molecule along the axes x and y. Unfortunately, even this quantitative approach does not necessarily allow the unambiguous determination of the zero-field splitting energy and its sign, which greatly hinders the identification of SMMs characterized by a negative D value large in magnitude. This is in part because the magnetometry in a direct current magnetic field is commonly performed using finely crystalline powders. For these samples, the magnetic susceptibility and the magnetization are averaged over all possible orientations of crystallites, thereby leading to the loss of considerable portion of data on their magnetic properties.

A possible approach to address this issue is to perform experiments on single crystals.[96] However, these studies are rather scarce [97] because of the difficulties of obtaining single

crystals of an appropriate size and also because the axes of magnetic anisotropy of individual molecules in the unit cell are often not parallel to each other as for example, in the monoclinic or orthorhombic crystal systems. However, these experiments are a challenge even for triclinic crystals. First, it is difficult to estimate in advance the directions of the axes of magnetic anisotropy in the molecule. Second, most magnetometers do not allow the crystal to rotate about an arbitrary axis. Although the magnetometry in a direct current magnetic field is necessary for investigations of SMMs, the results of simple static measurements of magnetization or magnetic susceptibility are insufficient to make a definite conclusion as to whether the compound under study is a promising SMM.

The magnetometry can be applied also for direct measurements of the spin-lattice relaxation time because SMMs display slow magnetic relaxation, which describes the time evolution of magnetization. A rather slow magnetic relaxation (tens of seconds or longer) is observed in efficient SMMs at helium temperatures. In the simplest version of these experiments (Fig. 13), samples are gradually cooled in a strong magnetic field H_1, which is usually sufficient to achieve the magnetization saturation at low temperatures. Then the external magnetic field is switched off and the time-dependent magnetization of the sample is measured. After the fitting of the results to an appropriate function (for example, to an exponential function), the magnetic relaxation time can be determined at a selected temperature.

An alternative approach to study the spin dynamics is illustrated in Fig. 14. The sample is cooled, then (time t_1) a weak dc magnetic field is applied and the temperature-dependent magnetization of the sample is measured. An increase in the temperature in the applied magnetic field leads to gradual magnetization of the sample until the equilibrium magnetization is reached at this temperature (time t_2), and the further heating does not cause changes in the magnetization. The repeated cooling of the sample (time t_3) in the magnetic field leads to an increase in the magnetization up to its full saturation (time t_4). In the final step, which is sometimes omitted, the magnetization is measured in the absence of magnetic field as a function of the temperature (Fig. 14, time t_5). This approach includes measurements under zero-field cooled (ZFC) conditions followed by cooling with an applied magnetic field (field-cooled, FC, conditions) and, therefore, is often called the ZFC/FC experiment. An important parameter of this experiment is the blocking temperature T_b, at which the maximum magnetization is achieved by heating the sample in the applied magnetic field (time t_2). When comparing the blocking temperatures of different SMMs, it should be taken into account that this temperature depends on the rate of the change in temperature during the ZFC/FC experiment and, as a consequence, on the performance characteristics of the magnetometer.

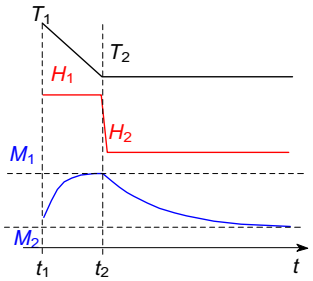


Figure 13. Plots of the temperature (black line), the magnetic field (red line) and the magnetization of the sample (blue line) *versus* the time in a standard time-resolved magnetometery experiment.

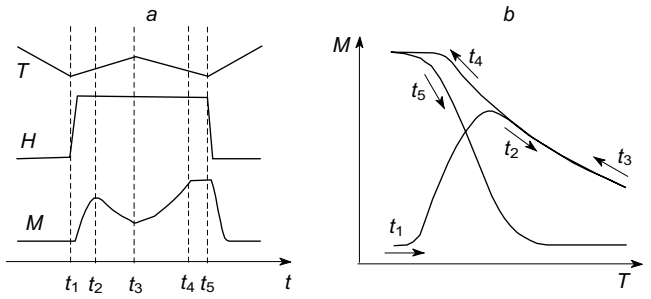


Figure 14. Plots of the temperature, the magnetic field strength and the magnetization of the sample *versus* the time (*a*) and the plot of the magnetization *versus* the temperature (*b*) in the ZFC/FC experiment. The sequence of events: up to the time t_1, the zero-field cooling of the sample; t_1, the switching of the external magnetic field and the onset of the gradual increase in the temperature; t_2, the establishment of the equilibrium value of magnetization; t_3, the beginning of the cooling of the sample under an external magnetic field; t_4, the saturation of magnetization; t_5, the switching off of the external magnetic field.

Finally, the most reliable method for revealing the SMM properties in the compound is based on applied field strength-dependent measurements of the magnetization. The cooling below the blocking temperature can give rise to magnetic hysteresis (see Fig. 8) indicative of remanent magnetization ($M \neq 0$ at $H = 0$). As in the ZFC/FC experiment, the blocking temperature depends on the measurement conditions, for example, on the magnetic field sweep rate (however, in all modern magnetometers this rate can be set as opposed to the rate of the change in temperature, which is much more difficult to control). This makes it possible to compare the data for different compounds, including those obtained in different experiments, and the presence of magnetic hysteresis is the most convincing evidence that the compound exhibits SMM properties. Despite high information power of time-resolved magnetometry in the dc magnetic field, these techniques can be used with confidence only if the magnetic relaxation time scale is comparable with the characteristic time of the method (tens and hundreds of seconds). Such long relaxation times are observed in SMMs only at very low temperatures.[98] Hence, these techniques cannot be applied to study in detail the faster spin dynamics.

Magnetometry in an alternating magnetic field (ac magnetometry) is an alternative to magnetometry in a dc magnetic field (dc magnetometry). Undoubtedly, this technique is the main method for investigation of SMMs. The observation of an unusual out-of-phase (imaginary) component of the magnetic susceptibility in a zero magnetic field for the mixed-valence Mn_{12} complex laid the foundations for the development of this area of single-molecule magnetism.[99] In ac magnetometry, the sample is placed in a weak (not stronger than 10 Œ) alternating magnetic field (sometimes in the presence of an external dc field). Hence, the magnetic moment of the sample is time-dependent. The corresponding dependence is detected using two receiving coils similar to those of the above-described gradiometers.

The major advantage of ac magnetometry over dc magnetometry is the simplicity of investigation of the spin dynamics of the system caused by changes in the frequency of alternating magnetic field. For example, at very low

frequencies, the magnetization depends on the applied magnetic field like in dc magnetometery, where the magnetic susceptibility is proportional to the angular coefficient of the plot of magnetization on the external magnetic field strength ($\chi_{ac} = dM/dH$). However, due to slow magnetic relaxation, an increase in the frequency of alternating magnetic field results in that the magnetization of the sample goes out-of-phase with respect to the external field strength. In other words, its spin dynamics may keep pace with changing external magnetic fields. This time lag is mathematically described by means of the magnetic susceptibility and the phase shift φ. The latter is the phase difference between oscillations of the applied magnetic field and the magnetization of the sample. In this case, the magnetization may be a complex value. Hence, the magnetic susceptibility is said to have an in-phase (real, χ') and out-of-phase (imaginary, χ'') components:

$$\chi' = \chi \cos \varphi \tag{20}$$

$$\chi'' = \chi \sin \varphi \tag{21}$$

Generally, the ac magnetometry data are represented as plots of χ' and χ'' *versus* the frequency of the alternating magnetic field for a particular set of temperatures (Fig. 15) or *versus* the temperature at selected frequencies of alternating field. If the magnetic relaxation time is τ, the condition $\nu\tau \ll 1$ is met at very low frequencies of magnetic field ν. In this case, the total magnetization is in phase with the oscillating magnetic field ($\chi'' = 0$), and the measured χ' value is the isothermal magnetic susceptibility (χ_T). At high frequencies ν , the spin system, on the contrary, does not have time to exchange the energy with the environment; the corresponding χ' value is called the adiabatic magnetic susceptibility χ_S. For intermediate frequencies ν, the following equations are valid:[96]

$$\chi'(\nu) = \frac{\chi_T - \chi_S}{1 + (\nu\tau)^2} \tag{22}$$

$$\chi''(\nu) = \frac{\nu\tau(\chi_T - \chi_S)}{1 + (\nu\tau)^2} \tag{23}$$

The presence of a maximum in the plot of the out-of-phase magnetization *versus* the frequency indicates that the sample shows slow magnetic relaxation under these conditions, the position of the maximum being related to the magnetic relaxation time as $\tau = 1/\nu$. Therefore, the results of measurements of the in-phase and out-of-phase components of magnetic susceptibility at several temperatures (see Fig. 15) can be employed to calculate the temperature dependence of the magnetic relaxation time. The analysis of this dependence using the above-described approaches provides the detailed data on the spin dynamics of the system.

If the magnetic relaxation occurs simultaneously *via* several mechanisms, there is a certain relaxation time distribution. In this case, the modified equations for χ' and χ'' can be applied

$$\chi'(\nu) = \chi_S + (\chi_T - \chi_S)\frac{1 + (\nu\tau)^{1-\alpha}\sin(\pi\alpha/2)}{1 + 2(\nu\tau)^{1-\alpha}\sin(\pi\alpha/2) + (\nu\tau)^{2-2\alpha}} \tag{24}$$

$$\chi''(\nu) = (\chi_T - \chi_S)\frac{(\nu\tau)^{1-\alpha}\cos(\pi\alpha/2)}{1 + 2(\nu\tau)^{1-\alpha}\sin(\pi\alpha/2) + (\nu\tau)^{2-2\alpha}} \tag{25}$$

where α is the parameter that takes into account the number of relaxation mechanisms: $\alpha = 0$ corresponds to the only Orbach process; at $\alpha > 0$, other mechanisms take place.

If several relaxation processes occur simultaneously, the Argand diagram[100] or, equivalently, the Cole – Cole plots[101] are considered as the preferable alternative representation of ac magnetometry results. These plots represent the dependence of the out-of-phase component of magnetic susceptibility χ'' on the in-phase component χ' (Fig. 16). At high α, the semicircle in the Argand diagram transforms to an arc in the case of a single relaxation processes. The more complex spin dynamics can manifest as a shift of the position of the maximum or the appearance of several maxima in Argand diagrams.

Generally, these diagrams are analyzed by the numerical fit of the experimental data to equations (24) and (25). This allows the determination of the dependence of the magnetic relaxation time on the external conditions (for example, on the temperature or the applied dc magnetic field) and then the evaluation of individual contributions of different mechanisms to the spin dynamics of the system. Unfortunately, a plenty of possible relaxation mechanisms makes this analysis very difficult due to the overparametrization.[54] For this reason, any additional data, which can decrease the number of unknowns in equation (17) and its analogues, provide invaluable assistance in the elucidation of the factors responsible for magnetic anisotropy of SMMs. These data can often be obtained by different spectroscopic methods.

4.2. Electron paramagnetic resonance spectroscopy

Electron paramagnetic resonance spectroscopy is based on the observation of energy absorption by a spin system *via* transitions between its levels. Depending on the approach applied, the measured absorption may be a function of either the external magnetic field (field-swept EPR) or the frequency of radiation (frequency-swept EPR). Field-swept EPR spectroscopy is applicable in the simplest case of a paramagnetic system with $S = 1/2$, when the externally

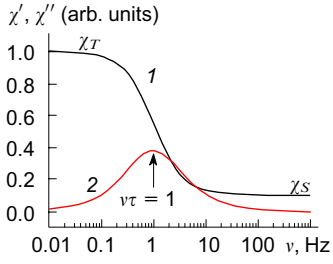


Figure 15. Plots of the in-phase component χ' (*1*) and the out-of-phase component χ'' (*2*) of magnetic susceptibility *versus* the frequency of the external magnetic field calculated using the following values of the parameters in equations (24) and (25): $\chi_T = 1$, $\chi_S = 1$, $\tau = 1$ and $\alpha = 0.2$. The arrow indicates the maximum of the frequency dependence of the out-of-phase magnetization.

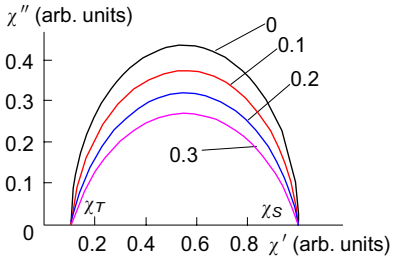


Figure 16. Argand diagrams calculated using the following values of the parameters in equations (24) and (25): $\chi_T = 1$, $\chi_S = 1$, $\tau = 1$ and α from 0 to 0.3.

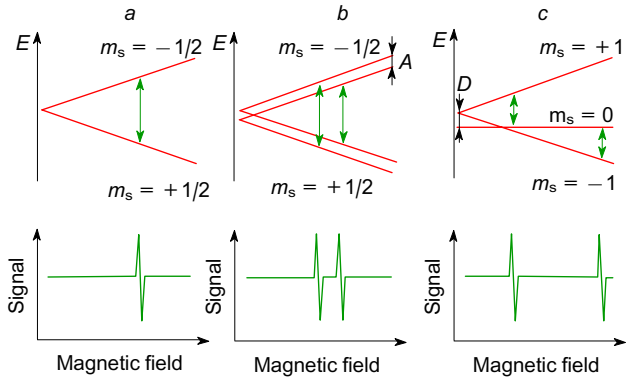


Figure 17. Schematic view of the splitting of energy levels due to the Zeeman effect and the related EPR spectra for a system with one unpaired electron (*a*), for an unpaired electron coupled with the nucleus with the spin 1/2 (*b*) and for a system with two unpaired electrons (*c*).

applied magnetic field leads to the removal of degeneracy of the spin levels followed by an increase in the splitting energy between these levels (Fig. 17 *a*). In this case, the interaction of the sample with electromagnetic radiation with the frequency ν leads to resonance energy absorption

$$\hbar\nu = g\mu_B B \qquad (26)$$

where g is the g-factor determined by the electronic structure of the compound and the presence of magnetic anisotropy, B is the magnetic field induction. For an electron, which does not interact with the environment (a free electron), the g-factor is 2.0023. However, unpaired electrons localized on molecular orbitals of chemical compounds experience different effects that affect the measured values of the g-factor, which is a second-rank tensor rather than a scalar quantity. Taking into account typical values of magnetic fields produced by electromagnets and superconducting magnets, samples are most often exposed to microwave radio frequency fields. The most commonly used EPR spectrometers operate at 9, 33 and 95 GHz (referred in the literature as X-, Q- and W-band EPR spectrometers, respectively). Equation (26) correctly describes the position of resonance absorption of a paramagnetic system with the spin $S = 1/2$ in the absence of magnetic anisotropy and electron–nuclear magnetic interactions. In this case, the position of the signal in the EPR spectrum is determined by the g-factor of the unpaired electron.

Generally, ions in an unsymmetrical environment show magnetic anisotropy, *i.e.*, the g-factor depends on the orientation of the spin system in a magnetic field. This anisotropic g-factor is usually represented as a second-rank tensor (g-tensor) with three principal values g_{xx}, g_{yy} and g_{zz} corresponding to the g-factor of the system in the externally applied magnetic field along the x, y and z axes of the g-tensor, respectively. If the ion is in an environment with axial symmetry, $g_{xx} = g_{yy} = g_\perp$, and two values, $g_\perp$ and $g_\parallel = g_{zz}$, are sufficient for the description of the g-tensor.

In the presence of magnetically active nuclei with a non-zero nuclear spin I, the EPR spectra of the molecules show additional splitting of energy levels (Fig. 17 *b*) due to electron–nuclear interactions. For example, the interaction of the unpaired electron with the ^{55}Mn nucleus ($I = 5/2$) causes the splitting of one EPR signal into six components with nearly equal intensity; for cobalt compounds, eight such lines can appear [$I(^{59}\text{Co}) = 7/2$]. The manifestation of an electron–nuclear interaction in the EPR spectra is referred to as hyperfine splitting. This splitting is quantitatively described by the hyperfine coupling constant A and the second-rank tensor **A** in isotropic and anisotropic cases, respectively.

The positions of energy levels in systems with several unpaired electrons ($S > 1/2$) are additionally determined by the zero-field splitting. The latter is described by the parameter D for systems with axial symmetry (Fig. 17 *c*). For ions with an odd number of unpaired electrons or with a half-integer spin (Kramers ions) in the absence of an external magnetic field, the energy levels, according to the Kramers theorem, are at least doubly degenerate ($M_s = \pm 1/2$, $\pm 3/2$, *etc.*; Fig. 18 *a*).[41] An important consequence of this theorem is the possibility to record EPR spectra for most of these ions because transitions between sublevels with $M_s = \pm 1/2$ (so-called intra-Kramers transitions) are always allowed by quantum mechanical selection rules. For non-Kramers ions, *i.e.*, for ions with an integer spin or with an even number of unpaired electrons, EPR spectra are difficult to measure because the energy sublevels with different $|M_s|$ values are distant in energy and transitions between levels with equal $|M_s|$ are forbidden for all M_s except $\pm 1/2$ (Fig. 18 *b*). Therefore, many field-swept EPR spectrometers, which are designed for investigation of systems with the spin $S = 1/2$, are not always suitable for studies of non-Kramers ions because of the impossibility of achieving the conditions of resonance absorption of electromagnetic radiation by the spin system.

Taking into account the above-mentioned interactions, the spin-Hamiltonian $\hat{H}$ of the system containing several unpaired electrons is described in a general form by equation (2), which is traditionally employed to interpret magnetometry data. In the presence of magnetically active nuclei in the molecule, their influence on the EPR spectrum shape can be taken into account by introducing an appropriate term into the spin-Hamiltonian

$$\hat{H} = D\left[\hat{S}_z^2 - \frac{S(S+1)}{3}\right] + E(\hat{S}_x^2 - \hat{S}_y^2) + \mu_B B g \hat{S} + \hat{S} A \hat{I} \qquad (27)$$

where A is the hyperfine splitting tensor and $\hat{I}$ is the nuclear spin operator. In accordance with the spin-Hamiltonian used, magnetometry and EPR spectroscopy provide a similar description of the systems in terms of magnetic anisotropy. However, the resonance character imparts spe-

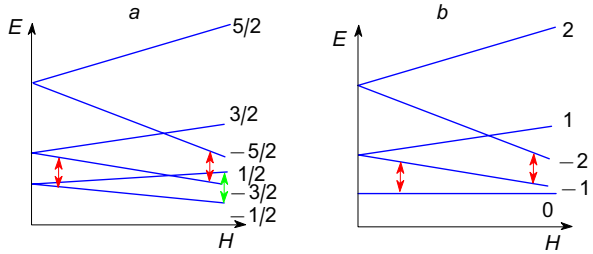


Figure 18. Schematic view of the energy levels for Kramers (*a*) and non-Kramers (*b*) ions with positive D. The red arrows indicate the transitions between sublevels with different $|M_s|$ values; green arrows, the transitions $(-1/2)-(+1/2)$.

cific features to EPR spectroscopy. Thus, resonance absorption of electromagnetic radiation by a spin system cannot be achieved for many SMMs using conventional X- and Q-band EPR spectrometers. When possible, EPR spectroscopy allows the evaluation of the parameters of the spin-Hamiltonian with high accuracy.

However, EPR spectroscopy cannot always be used for these purposes because some SMMs do not give an EPR signal.¶ This is due to the fact that the SMM properties are directly related to high magnetic anisotropy and a large M_s value of the system in the ground state. A key role is played by the ratio between the quantum energy of microwave radiation $h\nu$ in the selected frequency range and the zero-field splitting energy D. As a rule, if $|D| \gg h\nu$, it is impossible to observe EPR transitions in non-Kramers ions. In many transition metal complexes showing SMM properties, the D value varies from a few to hundreds of inverse centimeters, thereby limiting the application of conventional X- and Q-band EPR spectrometers ($h\nu = 0.3$ and 1.2 cm^{-1}, respectively). For example, in a cobalt(II) compound behaving as SMM ($S = 3/2$, the zero-field splitting energy is -100 cm^{-1}), transitions between the states of the ground Kramers doublet with $M_s = 3/2$ and $-3/2$ are forbidden by quantum mechanical selection rules ($\Delta M_s = 1$), and the energy of transitions between different Kramers doublets (for example, with $M_s = 3/2$ and 1/2; see Fig. 1 *d*) is in a terahertz range. In some cases, allowed transitions between the states of the upper Kramers doublet with $M_s = 1/2$ and $-1/2$ are not observed, because this doublet lies at a very high energy, resulting in its negligible population at helium temperatures, at which EPR spectra are usually recorded. Hence, the most promising SMMs, characterized by a huge negative zero-field splitting energy, have a number of properties, which make it impossible to record conventional EPR spectra.

In some cases, this issue can be addressed by applying a rather strong magnetic field, resulting in that the magnetic sublevels with $\Delta M_s = 1$ come closer to each other, thereby allowing the observation of transitions between these sublevels in standard frequency ranges (Fig. 19, position *1*).[102] Another situation may occur when the magnetic anisotropy is characterized by significant rhombicity with the result that M_s is not a good quantum number (*i.e.*, it is not the eigenfunction of the spin-Hamiltonian) due to the mixing of the states and, consequently, forbidden transitions become possible (Fig. 19, position *2*).[103 – 105]

¶ Such SMMs are also called EPR-silent.

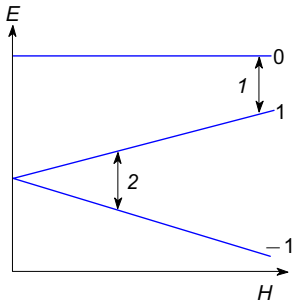


Figure 19. Schematics illustrating the possibility of the use of EPR spectroscopy for complexes with high magnetic anisotropy and negative D values: the observation of the transition in a very high applied magnetic field (*1*) and the formally forbidden transition (*2*). The numbers 0, 1 and -1 are the M_s values.

Finally, the heating of Kramers ions with a large negative zero-field splitting energy can give rise to an EPR signal due to the population of the upper Kramers doublet, in which transitions are allowed. For example, an increase in the temperature of a cobalt complex with $D = -40$ cm^{-1} above 40 K resulted in the appearance of a broad signal corresponding to transitions between the levels with $M_s = \pm 1/2$ (Fig. 20).[106] An analysis of the temperature dependence of the intensity of this signal for the cobalt complex provided the evaluation of the D value with high accuracy, which was later confirmed by other physical methods.[106]

The development of instruments for EPR spectroscopy of high-spin systems, which utilize very high microwave frequencies or very high magnetic fields,† is a challenge. Conventional EPR spectrometers are usually equipped with microwave resonators. The latter are special devices, which significantly enhance the sensitivity of the method at a fixed frequency of microwave radiation due to resonance effects. Such EPR spectra should be recorded in an alternating external field under continuous exposure of the sample to microwave radiation at a fixed wavelength. Besides, an increase in the frequency (decrease in the wavelength) of microwave radiation should be accompanied by a proportional decrease in the size of the resonator, thereby making it difficult and sometimes impossible to use this technique for very high frequencies (~200 GHz and higher). Finally, since not all transitions are usually observed for non-Kramers systems, the interpretation of these spectra is very challenging, and in some cases this problem can be addressed only by recording the spectra at different (in all cases, at very high) microwave frequencies. This technique,

† In the literature, both the terms high-frequency and high-field are used, which are often abbreviated as HF-EPR without indication of which particular parameter (frequency or field) has very high values.

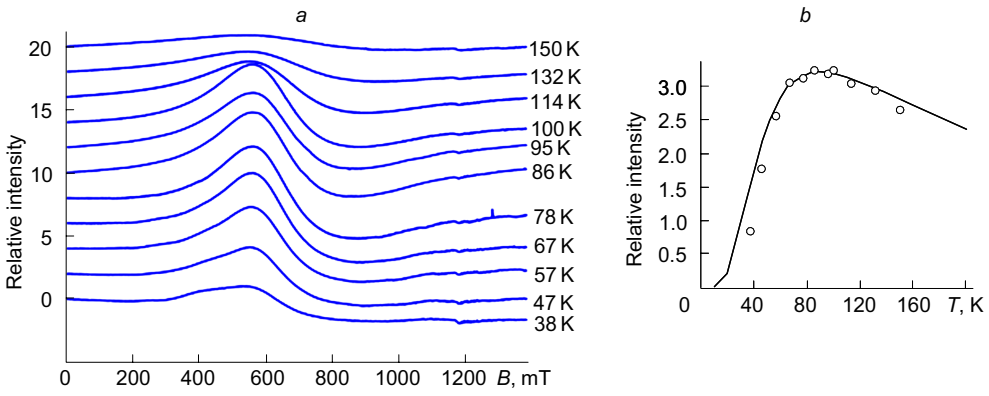


Figure 20. Q-Band EPR spectra of the complex $Co(GmCl_2)_3(BF)_2$ (where $GmCl_2$ is dichloroglyoxime) with $D = -40$ cm^{-1} in the case of thermal population of the excited Kramers doublet with $M_s = \pm 1/2$ (*a*) and the fitting of the temperature dependence of the integral intensity of the EPR signal by the Boltzmann distribution (*b*).[106] Reproduced with the permission of American Chemical Society.

called multi-frequency high-field EPR spectroscopy, proved to be a very valuable source of data in bioinorganic chemistry,[107] coordination chemistry[108] and molecular magnetism.[109] Unfortunately, the application of this technique in studies of SMMs is limited by the fact that the maximum frequency of available sources of microwave radiation, such as backward wave oscillators,[110] is not higher than 1.5 THz. The operating frequency of EPR spectrometers can be further increased using a free-electron laser as a source.[111–113] It should be noted that when using the magnetic field-swept EPR technique, the zero-field splitting energy is not, strictly speaking, directly measured but it is evaluated by the extrapolation of the D values determined at different applied magnetic fields.

The high-frequency EPR technique can also be used to record EPR spectra of SMMs with a large integer spin and relatively small $|D|$ ($|D| < h\nu$). For example, the application of a microwave frequency of 525 GHz for the complex Mn_{12} with $D = -0.46$ cm^{-1} made it possible to observe transitions between five lower Kramers doublets.[114] In another prime example of the use of EPR at ultrahigh frequency (968 GHz), four transitions between energy levels in a manganese complex ($S = 2$) were observed at very high magnetic fields (25 T).[102] The energy of these transitions (32.25 cm^{-1}) was much higher than the zero-field splitting energy, which demonstrates the applicability of high-frequency high-field EPR for measurements of the spectra of compounds with high magnetic anisotropy.

In recent years, the above-mentioned drawbacks have led researchers to develop an alternative approach, most often called the frequency domain magnetic resonance (FDMR), according to which EPR spectra are recorded by sweeping the frequency in microwave, submillimetre or terahertz ranges. Although this approach was proposed almost a half century ago,[115] it has attracted little attention until recently mainly due to the scarcity of powerful sources of radiation in the terahertz range.[116] Thus, a combination of several backward wave oscillators, each of which can be tuned over a certain narrow frequency interval, made it possible to span the frequency range from 30 GHz to 1.4 THz.[117] However, a further increase in the frequency is appropriate to do using modern IR spectrometers. Being a variant of far-infrared spectroscopy (FIR), this technique allows the observation of magnetic dipole transitions in a wide frequency range, but it is characterized by low sensitivity due to relatively small power of the radiation source.[116]

Another problem is that the frequency range, where magnetic dipole transitions typical of SMMs are observed, can contain spectral lines assigned to low-energy vibrational transitions. In order to distinguish between vibrational and magnetic dipole lines, the EPR spectra are recorded at different external magnetic fields. Since only transitions associated with zero-field splitting are sensitive to the magnetic field strength, the normalization of the data to the spectrum recorded at the maximum possible magnetic field allows the identification of magnetic dipole transitions. Thus, the subtraction of the spectrum recorded at zero magnetic field from the spectra recorded at magnetic fields varied from 1 to 11 T (Fig. 21 *a*) made it possible to unambiguously estimate the zero-field splitting energy at 230 cm^{-1} for a pseudotetrahedral cobalt complex.[118] An alternative approach to the normalization of the data obtained at different fields is based on the division of the spectra by the spectrum recorded at a particular magnetic field (Fig. 21 *b*).[119]

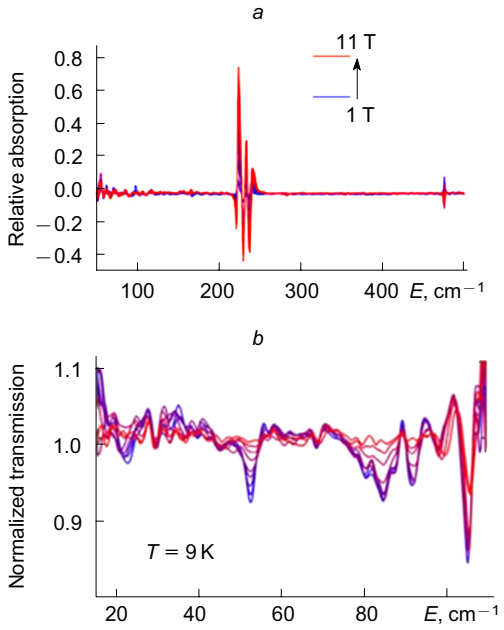


Figure 21. Far-infrared EPR spectra of the complex $[CoL_2][NHEt_3]_2$ (where L is 1,2-bis(methanesulfonamido)benzene), obtained by subtracting the zero-field absorption spectrum from the spectra measured in applied magnetic fields (*a*),[118] and the corresponding EPR spectra of the complex $\{C(NH_2)_3\}S[Er(CO_3)_4]\cdot 11\,H_2$, obtained by dividing the spectra measured in applied magnetic fields by the spectrum recorded at a field of 6 T (*b*).[119] Reproduced with the permission of Springer Nature and American Chemical Society.

Another example of the application of far-infrared spectroscopy to determine the structure of magnetic sublevels of the system is provided in experiments with the complex $Pr[Co(CN)_6]$,[120] which does not exhibit SMM properties by itself but it is a good system to demonstrate the applicability of different spectroscopic methods to determine the ligand field parameters in lanthanide complexes. The FIR spectra recorded at magnetic fields from 0 to 7 T show four magnetic transitions in the region from 20 to 100 cm^{-1} (Fig. 22 *a*). It should be noted that terahertz EPR (THz-EPR) spectrometers equipped with powerful backward wave oscillators as radiation sources allowed the identification of only two such transitions (Fig. 22 *b*), although with better resolution. Hence, it is important to use several spectroscopic methods to study the structure of magnetic levels of compounds with high magnetic anisotropy.

Far-infrared spectroscopy was applied to study a number of SMMs;[117] however, the results obtained by this method still raise a number of questions. The main question is why the spectra of some compounds show intense and rather narrow bands, whereas the signals of other structurally similar compounds are broad and not always can be separated from the baseline background.[117] For example, the signal corresponding to the double energy of zero-field splitting ($2|D|$) is clearly observedv[121] in the spectra of a trigonal prismatic cobalt(II) complex with the barrier to magnetization reversal of 205 cm^{-1}, but the intensity of this signal is quite low compared to the intensity of vibrational transition lines (Fig. 23 *a*). On the contrary, the spectrum of

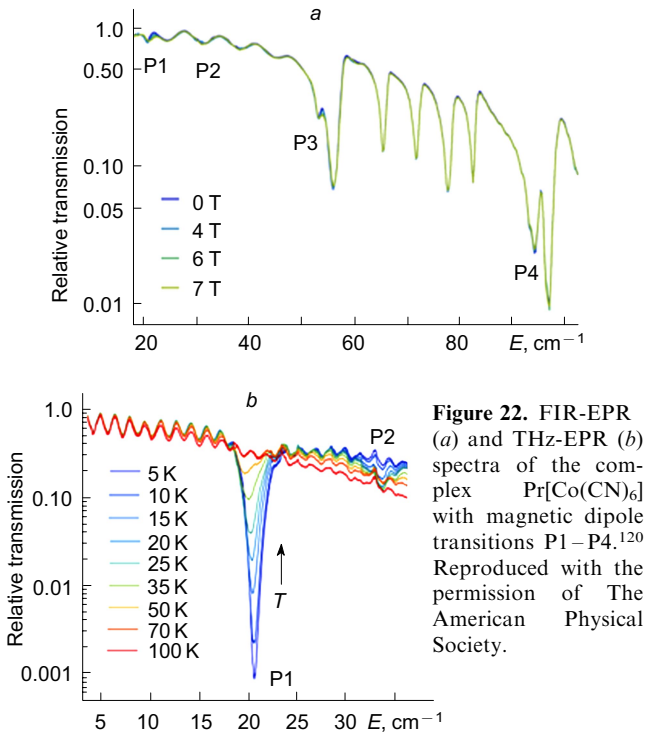


Figure 22. FIR-EPR (*a*) and THz-EPR (*b*) spectra of the complex $Pr[Co(CN)_6]$ with magnetic dipole transitions P1–P4.[120] Reproduced with the permission of The American Physical Society.

a cobalt(II) complex[122] with trigonal antiprismatic geometry and similar magnetic anisotropy shows an exceptionally intense signal (Fig. 23 *b*) and the nearly plane baseline, whereas this signal is absent in the spectra of complexes with geometry intermediate between a trigonal prism and a trigonal antiprism. To gain a deeper understanding of this fact, it is necessary to study in detail the spin–phonon coupling in SMM crystals using both spectroscopic methods and high-level quantum chemical calculations.[123]

Finally, a combination of different EPR techniques makes it possible to obtain results inaccessible when using only one of these techniques. For example, the combined use of far-IR spectroscopy and X-band EPR spectroscopy[124] or high-frequency EPR[125] resulted in a significant increase in the accuracy of determination of the spin-Hamiltonian parameters. The FDMR spectra provided a very accurate estimation of the zero-field splitting energy, while magnetic field-swept EPR spectroscopy ensured a high accuracy of determination of the g-tensor components. Separate mention should be made of studies, in which a synchrotron beam was employed as a terahertz radiation source in FDMR spectroscopy.[126] Thus, FDMR terahertz spectra were recorded with a very high signal-to-noise ratio, in particular, at the electron-storage ring BESSY II in

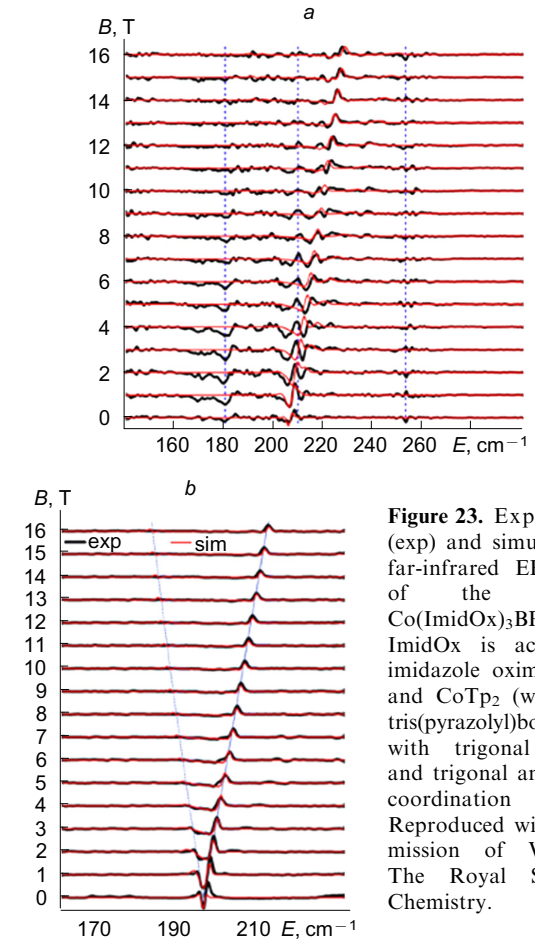


Figure 23. Experimental (exp) and simulated (sim) far-infrared EPR spectra of the complexes $Co(ImidOx)_3BPh$ (where ImidOx is acetylmethylimidazole oximate) (*a*)[121] and $CoTp_2$ (where Tp is tris(pyrazolyl)borate) (*b*)[122] with trigonal prismatic and trigonal antiprismatic coordination geometry. Reproduced with the permission of Wiley and The Royal Society of Chemistry.

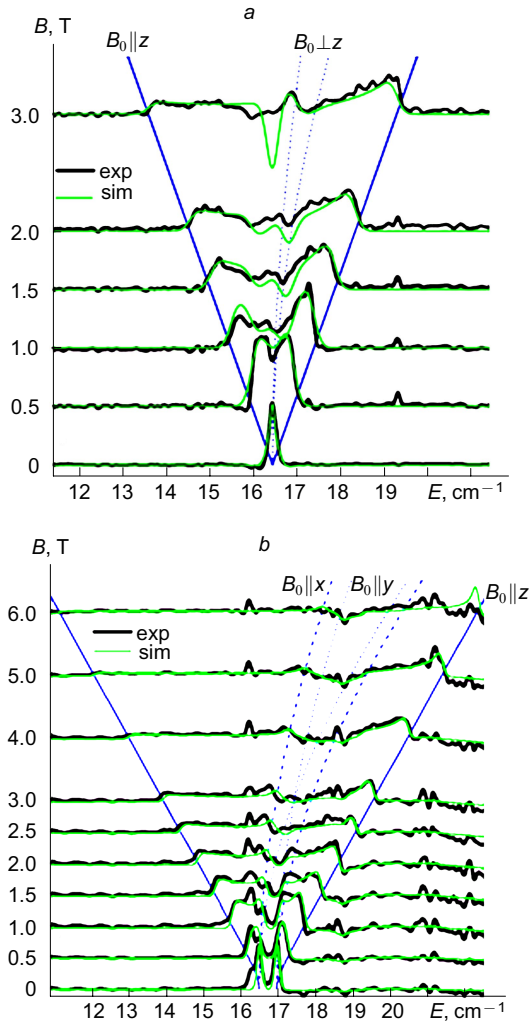


Figure 24. Experimental (exp) and simulated (sim) FDMR spectra of the complexes $[N(Bu^n)_4]Co^I(GmCl_2)_3(BPh)_2$ (*a*) and $[P(C_6H_5)_4]Co^I(GmCl_2)_3(BPh)_2$ (*b*).[128] Blue lines indicate the calculated energy level splitting for the perpendicular (dashed lines) and parallel (solid lines) orientations of the magnetic field with respect to the main molecular anisotropy axis. Reproduced with the permission of American Chemical Society.

Berlin,[126] due to the unprecedented intensity of the radiation source. In these experiments, the zero-field splitting energy and other spin-Hamiltonian parameters were determined with very high precision [127] from the dependence of the FDMR spectrum shape on the magnetic field. For example, the analysis of the spectra of two cobalt(I) complexes with d^8 electronic configuration ($S = 1$),[128] which differ only by the nature of the counterion (Fig. 24), revealed a significant difference in the rhombicity parameter of magnetic susceptibility. Besides, the zero-field splitting energy for these complexes was found to depend on the temperature. This fact may be attributed to both the temperature-induced change in the crystal packing parameters and the effect of weak intermolecular magnetic interactions. This is additional evidence that the spin dynamics in SMMs should be analyzed using the widest range of data obtained by a combination of different physical methods.

4.3. Optical spectroscopy

By optical spectroscopy is generally meant all spectroscopic methods working in the wavelength range from 5000 to 50000 cm^{-1}, *i.e.*, in the near-IR and Vis-UV regions. Since the absorption of optical photons leads to the population of excited states, including those caused by d–d and f–f transitions, the optical spectra recorded at rather low temperatures provide important information on the electronic structure of SMMs. Among optical spectroscopy techniques, luminescence spectroscopy, electronic absorption spectroscopy and magnetic circular dichroism spectroscopy are most commonly applied to investigate SMMs.

Luminescence spectroscopy, which is an indispensable tool for studying SMMs containing lanthanide or actinide ions,[129, 130] characterizes the structure of the ground electronic state. The spectra are recorded by the exposure of the sample to light of a particular wavelength, resulting in the population of the excited state. The system may return to the ground state *via* emission of a photon detected in the direction perpendicular to the excitation beam. According to Kasha's rule,[131] luminescence occurs from the lowest excited state (Fig. 25 *a*). Hence, luminescence spectra (Fig. 25 *b*) can be used to determine the splitting of the energy levels of the ground state, which is responsible for the magnetic behaviour of SMMs. For example, the energies of eight sublevels of the ground state of of a dinuclear dysprosium complex were estimated from the spectrum of this SMM in the region of $^4F_{9/2} \rightarrow {}^6H_{15/2}$ transitions, which contributed to an understanding of the nature of relaxation processes in the SMM.[132]

Another example of the successful use of luminescence spectra to determine the electronic structure of SMMs is the investigation of a heterodinuclear dysprosium zinc complex (Fig. 26).[133] For this complex, the energy of the first excited state (44.1 cm^{-1}) determined from the emission spectrum is very close to the barrier to magnetization reversal (35 cm^{-1}), which was determined by ac magnetometry most suitable for this purpose.[133] Besides, this energy is nearly equal to that for the diamagnetically diluted analogue,[134] the barrier height in which is 45 cm^{-1} due to a decrease in the contribution of alternative mechanisms of magnetic relaxation.

It is also worth noting that luminescence spectroscopy can be employed to reveal the dependence of the energy of magnetic sublevels on the applied magnetic field. For

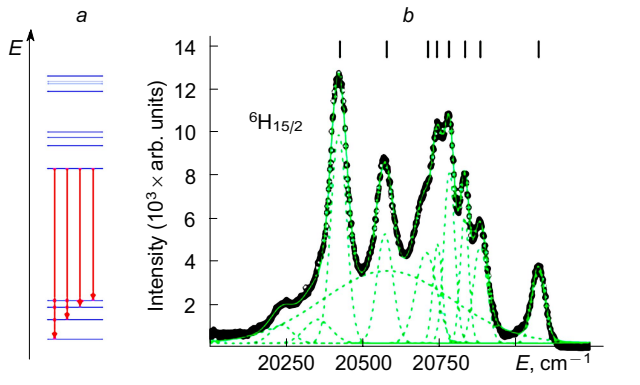


Figure 25. Schematic view of the use of luminescence spectroscopy to determine the electronic structure of the ground state of SMMs (*a*) and the experimental luminescence spectrum of Dy_2(bpm)$(fod)_6$] (bpm is 2,2′-bipyrimidine, Hfod is 6,6,7,7,8,8,8- heptafluoro-2,2-dimethyloctane-3,5-dione) [132] belonging to the $^4F_{9/2} \rightarrow {}^6H_{15/2}$ transition upon irradiation at a wavelength of 341 nm at 5 K (solid line) and its fitting with a set of Gaussian functions (dashed lines) (*b*). The vertical lines above the spectrum correspond to the evaluated energy levels. Reproduced with the permission of The Royal Society of Chemistry.

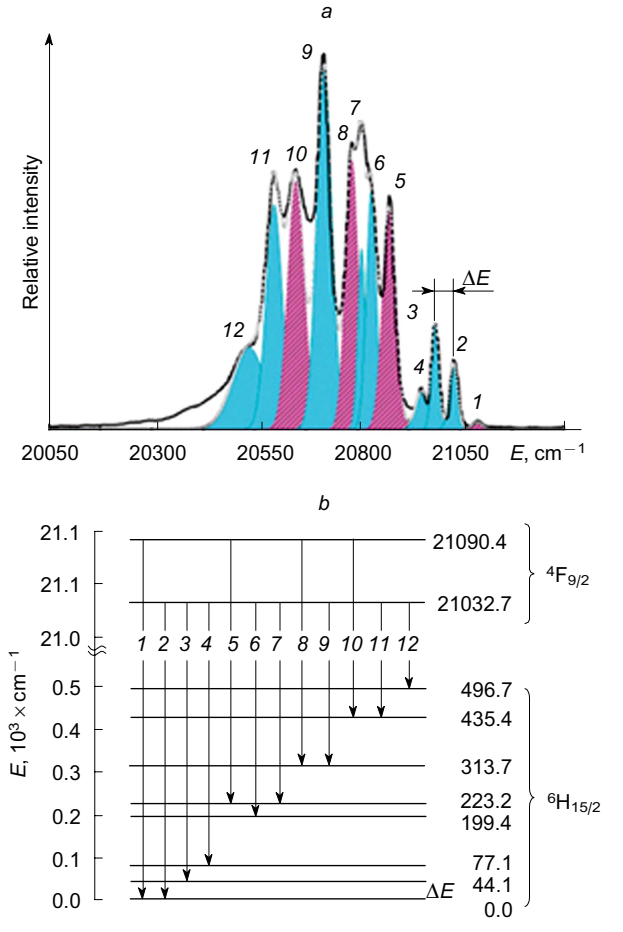


Figure 26. Emission spectrum of the complex $Zn(NO_3)LDy(NO_3)_2(H_2O)$], where H_2L is *N*,*N*′-bis(3-methoxysalicylidene)-1,2-diaminoethane), (*a*), and the magnetic level structure for the ground state calculated from this spectrum (*b*).[133] The assignments of the signals to transitions between energy levels are indicated by positions *1*–*12*. Reproduced with the permission of The Royal Society of Chemistry.

example, the externally applied magnetic field can cause the splitting of the bands in the emission spectra or their shift,[135] thereby providing information complementary to that derived from high-frequency EPR spectra. Although the effect of the magnetic field on the positions of the lines in luminescence spectra is known for more than a half century,[136] there are scarce examples of molecular compounds studied by this method. Nevertheless, taking into account the growing popularity of multifunctional materials combining luminescence and SMM properties,[137] it can say with certainty that the number of such studies will be increased.

The data on the structures of the excited states of SMMs, which cannot be derived from luminescence spectra, can be obtained using electronic absorption spectroscopy at very low temperatures, at which only the lowest level of the ground state is populated. The photon absorption will give rise to a spectrum, the analysis of which will provide a detailed knowledge of the electronic structure of the excited state. Since the observed f → f transitions are forbidden by the Laporte rule,[138] their intensity is low. However, due to a small width, the lines can be detected despite insignificant extinction coefficients.[139]

Electronic absorption spectroscopy can also be used to study the electronic structure of the ground state of SMMs.[120] For this purpose, the spectra should be recorded at several temperatures. A change in the temperature allows the sequential population of magnetic sublevels of the ground state. For example, only a line corresponding to the transition between the ground states of the multiplets $^3H_4$ and $^3P_0$ was observed for the complex $Pr[Co(CN)_6]$ at 5 K. A gradual increase in the temperature led to the sequential population of the higher-lying sublevels (Fig. 27 *a*) and the appearance of additional signals in the spectrum (Fig. 27 *b*). Although the accuracy of determination of the corresponding energies by electronic absorption spectroscopy is generally lower than that using THz-EPR or far-IR spectroscopy, the former method is commonly applied to study the structure of the ground state.

Magnetic circular dichroism spectroscopy is another important optical spectroscopy technique extensively used to study the magnetic properties. It arises from the differential absorption of right- and left-handed circularly polarized light in the presence of a magnetic field applied parallel to the light beam. The scope of application of this method is not limited to chiral compounds because it is based on the Faraday effect, *i.e.*, the rotation of the plane of polarization of linearly polarized light when it passes through an optically inactive compound in the applied magnetic field.

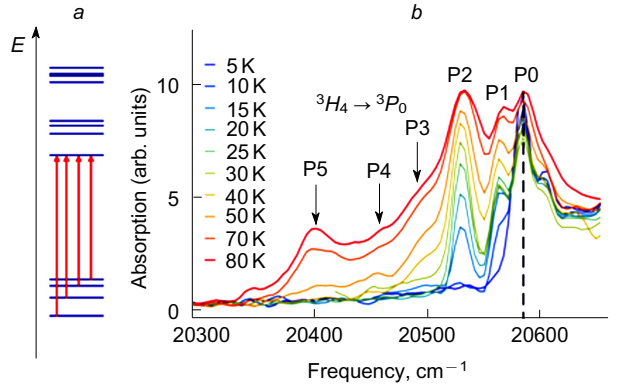


Figure 27. Schematic view of the use of electronic absorption spectroscopy to study the electronic structure of the ground state of SMMs (*a*) and the experimental absorption spectrum of the complex $Pr[Co(CN)_6]$ in the temperature range of 5 – 80 K at zero magnetic field (*b*).[120] P0 – P5 are magnetic transitions. Reproduced with the permission of American Physical Society.

In the general case,[140] the difference in the light polarization with different polarization states (so-called differential absorption ΔA) depends on the corresponding terms of magnetic circular dichroism

$$\frac{\Delta A}{E} = \sigma\mu_B H\left[A\left(-\frac{\partial f(E)}{\partial E}\right) + Bf(E) + \frac{Cf(E)}{kT}\right] \qquad (28)$$

where σ is a set of spectroscopic constants, $f(E)$ is the function describing the line shape, A, B and C are three terms. The term A takes a non-zero value, when the applied magnetic field removes the degeneracy of the excited state, resulting in the difference in the energy of absorption of right- and left-handed circularly polarized light (Fig. 28 *a*) and, consequently, in the appearance of a temperature-independent signal as a dispersion in the magnetic circular dichroism spectrum. Since transitions occur from the same level of the ground state, the signals of left- and right-handed circularly polarized light have identical intensity and the shape of the line corresponding to the term A is described by the simple Lorentzian function. The term B arises from the mixing of individual states in an external magnetic field. The mixing is observed only in terms of the second-order perturbation theory and leads to rather weak signals as the adsorption (Fig. 28 *b*).

The term C, which plays the most important role in SMMs,[141] appears in the case of the degenerate ground state split by an external magnetic field. The difference in the Boltzmann population of magnetic sublevels results in that the absorption of light with different polarization at the levels with different energy occurs with different intensity. In this case, the signal in the magnetic circular dichroism spectrum has a characteristic shape described as the difference between two Lorentzian functions with different posi-

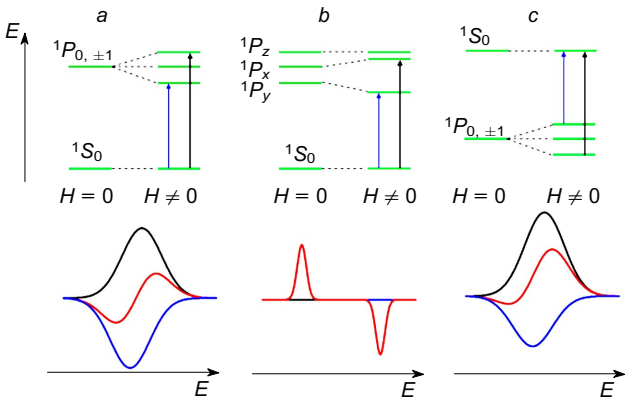


Figure 28. Schematic view of the terms in the magnetic circular dichroism spectrum. The term A is defined by the degenerate nature of the excited state (*a*), the term B arises from the mixing of the states caused by the applied magnetic field (*b*), the term C is related to the degenerate nature of the ground state (*c*). The magnetic circular dichroism spectrum is shown as red lines; the absorption of left-handed circularly polarized light, as black lines; the absorption of right-handed circularly polarized light, as blue lines.

tions of the maxima and intensities (Fig. 28 *c*). Since the populations of the resulting Zeeman sublevels additionally depend on the temperature, the observed asymmetric signals have a characteristic temperature dependence.[142] This dependence is often analyzed together with the analysis of the plot of the signal in the magnetic circular dichroism spectrum *versus* the applied magnetic field, thereby enabling the detailed description of the electronic structure of the ground state of SMMs.[120]

Magnetic circular dichroism spectroscopy is a rare tool suitable for investigation of the electronic structure of SMMs both in the ground and excited states. Therefore, this method is exceptionally important in studies of SMM properties. For example, the data obtained by this method excellently complement the EPR and electronic absorption spectroscopy data. Another advantage of magnetic circular dichroism spectroscopy is that it allows the determination of not only the relative energies of individual electronic states but also the wavefunctions that contribute to these states.[120] These data are of invaluable assistance in the explanation of the characteristic features of the spin dynamics in SMMs, because modern calculation methods using these data enables the evaluation of the probability of a particular magnetic relaxation mechanism.[132] An additional advantage of magnetic circular dichroism spectroscopy is that it can be applied to study isolated SMM molecules in solutions and on the surface. For practical applications of SMMs in devices for data storage and processing, it is necessary that SMM properties of the isolated molecule on the surface be retained. For example, the analysis of the temperature and field dependences of the signals in the magnetic circular dichroism spectrum (Fig. 29 *a*) made it possible to observe for the first time the magnetic hysteresis for an individual Mn_{12} molecule, measure the magnetic relaxation times (Fig. 29 *b*) and demonstrate the retention of QTM in solution.[143]

4.4. Nuclear magnetic resonance spectroscopy

Nuclear magnetic resonance (NMR) spectroscopy, which is widely used to study diamagnetic compounds, is mistakenly considered inapplicable to paramagnetic compounds, although the foundations for the use of NMR for this purpose were laid already at the dawn of development this technique.[144] Until recently, the application of NMR spectroscopy of paramagnetic compounds, which is sometimes referred to as paramagnetic NMR spectroscopy, was limited to investigation of shift agents, which generally contain paramagnetic lanthanide ions,[145, 146] for the determination of the structures of biomacromolecules in structural biology[147, 148] and relaxation agents or temperature and pH sensors[149–151] for magnetic resonance imaging in medical diagnostics.[151–153] Meanwhile, due to a sharp increase in the number of studies of molecular magnetic materials in the past two decades, this method has attracted attention as a tool for investigating SMMs. Unlike EPR or optical spectroscopy, which can be used to measure the energy difference between magnetic sublevels of the ground state, the transitions in the NMR spectra are in a radically different frequency range and the effect of the paramagnetic center on the positions of the corresponding signals is of nonlinear character. Besides, NMR spectroscopy of finely crystalline samples of paramagnetic compounds or their solutions frozen at very low temperatures (traditionally used in the above-described spectroscopic techniques) presents a number of technological and methodological challenges.[92] Hence, attempts to use NMR spectroscopy to investigate SMMs include only the standard (in organic and coordination chemistry) measurements of the spectra of solutions at nearly room temperatures,[154] and the available approaches are in essence more similar to magnetometry than to other spectroscopy techniques.

One of the main results of dc-magnetometry is the temperature dependence of magnetic susceptibility, most often, its isotropic value averaged over all orientations of the molecules in the crystalline sample in the applied magnetic field. This value in solution can be obtained by NMR spectroscopy in terms of the Evans method[155] based on the simultaneous measurement of NMR spectra of two solutions generally using two coaxial NMR tubes. One tube is filled with a solvent supplemented with an additional standard compound (most commonly, tetramethylsilane, TMS), and another tube contains the paramagnetic analyte with a known concentration (Fig. 30). The presence of a paramagnetic dopant in the latter solution leads to a change in its magnetic susceptibility, with the result that the chemical shifts of TMS in the inner and outer tubes are different. The observed difference can be related to the molar magnetic susceptibility of the analyte.

Despite the simplicity of this method, which can be used to measure NMR spectra in a wide temperature range, the accuracy of the determination of χ_m by this method is not quite high.[156] Some contributions to the error of measurements of the molecular magnetic susceptibility by the Evans method can be compensated using a more complicated scheme for the data processing compared to that presented in Fig. 30. For example, the mass magnetic susceptibility of the solvent and the dependence of its density on the temperature can be taken into account[157]

$$\chi_m = \frac{\Delta\delta M}{v_0 S_f c} + \chi_0 M + \frac{\chi_0(d_0 - d_s)M}{c} - \chi_m^{dia} \qquad (29)$$

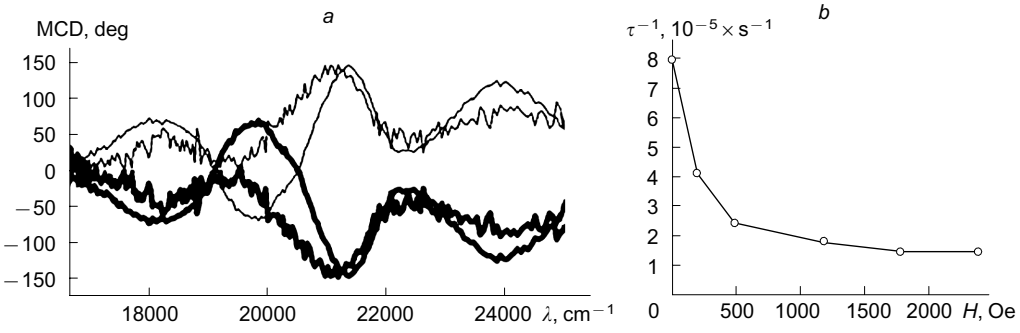
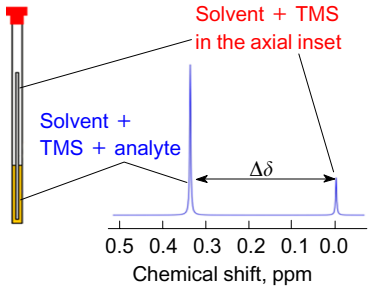


Figure 29. Magnetic circular dichroism (MCD) spectra of solutions of Mn_{12} in dichloromethane : toluene (1 : 1, black lines) and acetonitrile : dimethylformamide (1 : 2, gray lines) mixtures (*a*) and the plots of the magnetic relaxation rate *versus* the applied magnetic field strength at 4 K (*b*).[143] Reproduced with the permission of American Physical Society.



$$\chi_m = \frac{\Delta\delta\, M}{\nu_0\, S_f\, c} - \chi_m^{dia}$$

Figure 30. Schematic view of the application of the Evans method to determine the molar magnetic susceptibility of a solution of the paramagnetic compound by NMR spectroscopy. The following designations are used: χ_m is the molar magnetic susceptibility, M is the molecular mass of the paramagnetic compound, χ_m^{dia} is the diamagnetic component of the molar magnetic susceptibility calculated based on Pascal s constants,[158] $\Delta\delta$ is the chemical shift difference, ν_0 is the Larmor frequency of the magnet, S_f is the parameter that depends on the geometry of the magnet ($4\pi/3$ for standard superconducting magnets with a vertical coil), c is the concentration of the paramagnetic compound.

where d_0 and d_s are the density of the pure solvent and the solution, respectively.

However, in this case, the difficulties with the determination of the exact concentration of paramagnetic compounds is the main source of errors in the Evans method because even an insignificant evaporation of the solvent at room temperature or the presence of a small impurity in the analyte can lead to substantial deviations of the results of measurements from the expected values.

The NMR spectra thus measured are an analogue of the results of dc-magnetometry for finely crystalline samples. Nevertheless, since the magnetic susceptibility is a tensor, its averaging

$$\overline{\chi} = \frac{\chi_{zz} + \chi_{yy} + \chi_{xx}}{3} \tag{30}$$

is accompanied by the loss of important data on magnetic anisotropy, which is a key characteristic of SMMs.

In the case of solutions at room temperature, NMR spectra are also formally recorded for an isotropic sample; however, the positions of the lines in the corresponding spectra described by chemical shifts depend on the anisotropic parameters of the magnetic susceptibility tensor

$$\Delta\chi_{ax} = \chi_{zz} - \frac{\chi_{yy} + \chi_{xx}}{2} \tag{31}$$

$$\Delta\chi_{rh} = \chi_{yy} - \chi_{xx} \tag{32}$$

where χ_{ax} and χ_{rh} are the axial anisotropy magnetic susceptibility and its rhombicity, respectively.

The presence of a paramagnetic ion in the chemical compound leads to the shift of the signals of all its nuclei in the NMR spectra due to their hyperfine coupling with unpaired electrons. The shift can be described by the sum of the isotropic contact contribution, arising from the electron density redistribution for the unpaired electron (or the spin density) from the paramagnetic ion to the nuclei of the molecule, and the pseudocontact contribution due to dipole–dipole interactions between the nuclear magnetic moments and the unpaired electron.

The isotropic contact contribution, which is also termed the Fermi contact, causes the contact shift (δ_{cs}) of all signals in the NMR spectrum, which is proportional to the spin density on the nucleus (ρ)

$$\delta_{cs} = \frac{\mu_0 \mu_B^2 g^2 S(S+1)}{9kT}\rho \tag{33}$$

Equation (33) is based on a number of assumptions, which are not always valid,[159] thereby significantly complicating the interpretation of NMR data in the cases of a large contact contribution. Generally, this contribution quite rapidly drops with increasing distance from the paramagnetic nucleus and becomes negligible at the distance longer than five covalent bonds.

On the contrary, the pseudocontact contribution (δ_{pcs}), due to its dipole–dipole nature, can affects the chemical shifts of the atoms located at much longer distances from the paramagnetic ion. However, this contribution directly depends on the spatial arrangement of the atoms, *i.e.*, on the structure of the paramagnetic compound

$$\delta_{pcs} = \frac{1}{12\pi r^3}\left[\Delta\chi_{ax}(3\cos^2\theta - 1) + \frac{3}{2}\Delta\chi_{rh}(\sin^2\theta \cdot \cos 2\varphi)\right] \tag{34}$$

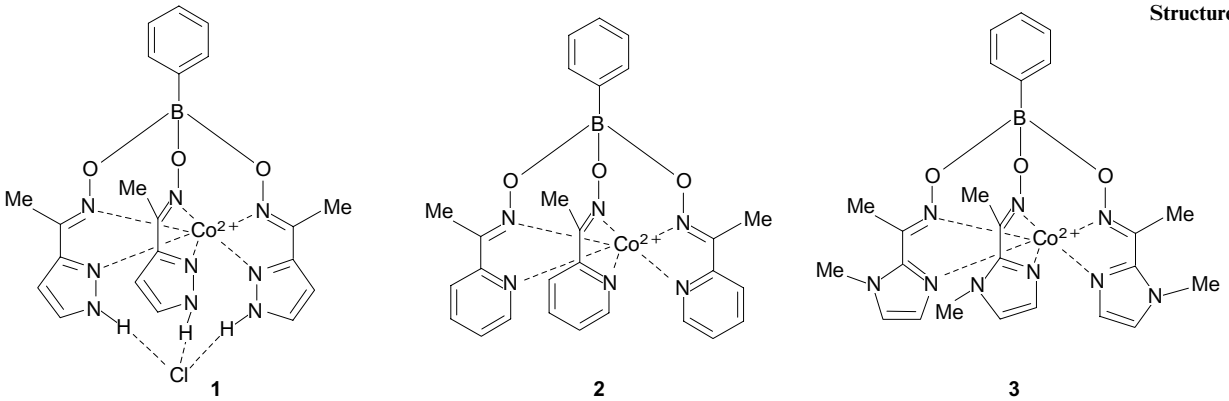
where r, θ and φ are the spherical coordinates of the nucleus in the systems of coordinates of the magnetic susceptibility tensor of the paramagnetic ion. Equation (34) is generally used to determine the structure of biological macromolecules using a paramagnetic probe;[160] this equation is considerably simplified for the axial symmetry of this probe

$$\delta_{pcs} = \frac{1}{12\pi r^3}\left[\Delta\chi_{ax}(3\cos^2\theta - 1)\right] \tag{35}$$

If the structure of the corresponding paramagnetic complex is known, the analysis of the NMR spectra allows the determination of the anisotropic parameters of the magnetic susceptibility tensor, therefore serving as an analogue of the more labor intensive of single-crystal dc-magnetometry. Besides, NMR spectroscopy can be used to determine the g-tensors, the zero-field splitting energy, the ligand field parameters for lanthanide compounds, *etc.*, because the components of the magnetic susceptibility tensor are related to the energy levels and, correspondingly, to the parameters of the corresponding Hamiltonian by the Van Vleck equations.[161] For example, the simultaneous use of magnetometry and NMR spectroscopy to study a series of well-known SMMs based on lanthanide phthalocyanine complexes[71,162] resulted in a significant increase in the accuracy of the determination of the ligand field parameters compared to the results obtained separately by each method.

Since the isotropic magnetic susceptibility, as well as its anisotropic parameters, for SMMs depend on the temperature, the measurement of NMR spectra in a wide temperature range for SMMs allows the determination of the temperature dependence of pseudocontact shifts $\delta_{pcs}(T)$. Using this dependence and equation (35), one can evaluate $\Delta\chi_{ax}(T)$ for complexes with axial symmetry of the coordination environment or $\Delta\chi_{ax}(T)$ and $\Delta\chi_{rh}(T)$ for lower-symmetry complexes, provided that the three-dimensional structure of paramagnetic complex is known (for example, from the X-ray diffraction data or quantum chemical calculations).

Structures 1 – 3



1 **2** **3**

Apart from contact and pseudocontact contributions to the chemical shifts, the NMR spectra of paramagnetic compounds contain the diamagnetic contribution (δ_{dia}), which can be related to the corresponding chemical shifts of an appropriate diamagnetic analogue, such as an isostructural complex with a diamagnetic metal ion [for example, zinc (II) or iron(II) in a low-spin state], or even of a free ligand

$$\delta_{exp} = \delta_{dia} + \delta_{cs} + \delta_{pcs} \quad (36)$$

In this equation, the contact contribution depends on the isotropic hyperfine coupling constant and, as a consequence, on the distribution of the spin density in the molecule, which can be determined from quantum chemical calculations, for example, in terms of density functional theory (DFT). In the case of lanthanide complexes, the δ_{cs} value can generally be ignored due to the weak involvement of f-electrons in the binding to ligands, which does not lead to a significant delocalization of the spin density from the paramagnetic metal ion to the ligand,[144] as opposed to d-transition metal complexes. However, since there are exceptions from this rule,[163] the decision of whether it is necessary to take into account the contact contribution should be taken for each particular type of paramagnetic metal complexes.

Therefore, measurements of NMR spectra of SMMs in a wide temperature range accessible for the solvent use (for example, from 220 to 320 K) followed by the fitting of the observed chemical shifts fitting with equation (35) taking into account the diamagnetic and contact contributions allow the determinations of the temperature dependence $\Delta\chi_{ax}(T)$ and, consequently, the zero-field splitting energy or the ligand field parameters and the corresponding barrier to magnetization reversal. In the case of SMMs containing paramagnetic lanthanide ions, these approaches, which differ only by the type of the spin-Hamiltonian, were successfully applied to investigate phthalocyanine [164 – 166] and porphyrin complexes,[167] double-decker cyclooctatetraene complexes [168] and heterospin complexes with stable organic radicals.[169]

Examples of investigation of paramagnetic first-row transition metal complexes by NMR spectroscopy are much more rare. This is due to the fact that these ions are characterized by very long electronic relaxation times and related short nuclear relaxation times for magnetic nuclei, resulting in a significant broadening of NMR lines up to their complete disappearance. Besides, first-row transition metals have much lower magnetic anisotropy compared to lanthanides. It is worth noting that there are first-row

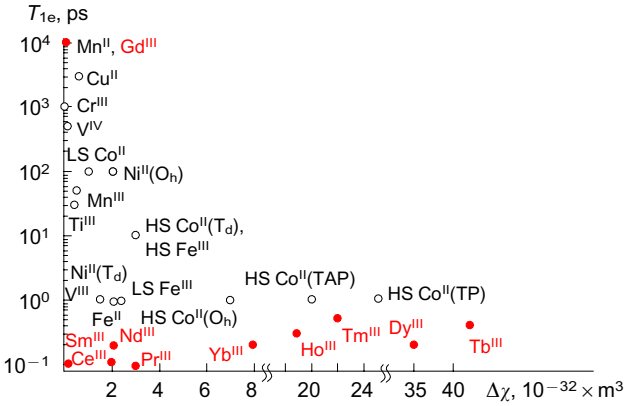


Figure 31. Typical electronic relaxation times (T_{1e}) and the anisotropy of the magnetic susceptibility tensor ($\Delta\chi$) for lanthanide and first-row transition metal ions.[154] The following designations are used: HS is high-spin, LS is low-spin, TP is a trigonal prism, TAP is a trigonal antiprism. Reproduced with the permission of INEOS OPEN.

transition metal complexes, which combine high magnetic anisotropy and short electronic relaxation times (Fig. 31); however, a range of such complexes are largely limited mainly to high-spin cobalt(II) complexes. For example, NMR spectroscopy was used for the preliminary evaluation of the magnetic anisotropy of a series of cobalt(II) cage complexes (structures **1** – **3**) and, consequently, for the assessment of their potential of SMMs.[121, 170 – 172] The corresponding values determined from the analysis of the temperature dependence of the chemical shifts in NMR spectra rather adequately reproduce the results of other spectroscopic methods and, importantly, magnetometry.

Nuclear magnetic resonance spectroscopy of paramagnetic compounds provides wide possibilities for the screening of potential SMMs. However, it has limitations. First, equation (34), rather than (35), should be used for metal complexes, the symmetry of which is lower than axial, which may require (particular, in the case of lanthanide compounds) the inclusion of higher-order anisotropic terms.[173] Second, equations (34) and (35) are based on Bleaney's model [144] and the central ion model,[174] which postulate that the distance to the paramagnetic center is rather large and the pseudocontact contribution is due to the interaction between the magnetic nucleus and the spin density localized on the metal ion. The delocalization of the unpaired electron density to the ligand can also be described using

the results of quantum chemical calculations of contact shifts.[175] Third, the Van Vleck equation underlying approaches to the quantitative interpretation of NMR spectra of paramagnetic compounds does not take into account the orbital momentum unquenched by the ligand field. Therefore, this equation cannot be applied for systems with the degenerate ground state, which should be described using of complex spin-Hamiltonians, which directly take into account the contribution of the spin – orbit coupling.[122] Finally, it is necessary to take into account that the structure of the compound in solution may significantly differ from the structure in the crystal (determined by X-ray diffraction), and the crystal packing effects may dramatically change the characteristics of SMMs.[176] Besides, for solutions of conformationally flexible compounds, it is necessary to take into account the possible molecular dynamics on the NMR time scale, which can lead to the complete or partial averaging of paramagnetic shifts.[177] Measurements of NMR spectra in coordinating solvents can also lead to significant changes in the structure of the complex and its magnetic properties.[124] Nevertheless, these drawbacks not detract from the advantages of NMR spectroscopy over other spectroscopic techniques and magnetometry methods, such as its wide availability, the possibility of detecting minor amounts of the compound of interest and no need in the thorough purification or isolation from the reaction mixture.[178] Hence, the analysis of the temperature dependence of chemical shifts in the NMR spectra is indispensable for the preliminary evaluation of the potential of various metal complexes as SMMs.

4.5. X-Ray diffraction

Among diffraction methods of investigation of matter, only X-ray diffraction is widely used to study SMMs, the properties of which are generally measured in the crystalline state.[179] Although single-crystal polarized neutron diffraction provides information on the spin density distribution,[180] which directly determines the magnetic properties of the compound (for example, local magnetic anisotropy of a paramagnetic ion [181, 182]), strict requirements imposed on the quality of the sample (the main requirement is that the single crystal should be of large size that is difficult to achieve), make this method inaccessible to most of SMMs.[181] On the contrary, due to recent advances in the design of new X-ray sources and detectors,[183] X-ray diffraction has gained wide acceptance in institutions for chemistry to determine the atomic molecular structures of crystals of different nature and size. Besides, X-ray diffraction is based on X-ray scattering by electrons and allows the determination of not only atomic coordinates but also the electron density distribution [184] related to various properties of the system in the ground state (according to the Hohenberg – Kohn theorem).[185]

However, in most cases, X-ray diffraction studies of SMMs is limited to investigation of the molecular structures of several complexes, which differ in the nature of the ligand [186] or the counterion.[187] This makes it possible (with varying degrees of success [188]) to reveal the dependence of the characteristics of SMMs (magnetic anisotropy,[189] the zero-field splitting energy,[142, 190, 191] the barrier to magnetization reversal [54, 187, 192] or the contributions of different mechanisms to magnetic relaxation [54, 187, 189]) on the geometry of the coordination environment of the metal ion. For example, in a series of iron(II) complexes, which display a magnetic relaxation under an applied magnetic field, the deviation from the linear geometry causes a decrease in the magnetic anisotropy and the barrier to magnetization reversal [54] due to the deviation from the axial symmetry and the Renner – Teller effect.[58] On the contrary, equally high magnetic anisotropy was observed in six-coordinate cobalt(II) complexes with both a trigonal prismatic ($\varphi = 0$) [176, 193] and a trigonal antiprismatic geometry [122, 189] ($\varphi = 60°$). However, due to quantum tunneling of magnetization, the latter complexes exhibit SMM properties under an applied magnetic field. In the case of an intermediate geometry ($0 < \varphi < 60°$), the anisotropy was much lower [194] and these complexes were poor SMMs even under an applied field.

Generally, these studies are performed using X-ray diffraction data for different samples at the same temperature (most often, at liquid nitrogen temperature, at which slow magnetic relaxation was observed only once [22]) under atmospheric pressure. Therefore, it is impossible to relate the structure to the magnetic properties measured under the same conditions for one compound with the same set of intermolecular interactions, which have an unpredictable effect on the behaviour of SMMs in the crystalline state.[176, 189] There are examples when the observed characteristics of SMMs (in particular, the barrier to magnetization reversal) were adequately explained by characteristic features of their crystal structures (for example, by the size of the substituent in the alcohol solvent molecule in the crystal solvates of the same SMM).[195] However, the magneto-structural correlations, which were formulated for individual classes of SMMs based on the analysis of the X-ray diffraction data for several representatives of the appropriate series are much less reliable and have a weaker predictive power compared to correlations, which can be obtained using high-level quantum chemical calculations. The latter can be used to generate a set of structures with desired geometry, thereby making it possible to reveal the effect of any changes on the SMM properties.[26, 196, 197] Evident drawbacks of this method are the observation of structural distortions, which may be absent in real SMMs.

One way of addressing this issue is the use of X-ray diffraction data obtained from one crystal at different temperatures.[198] The corresponding set of real structures with slight structural changes caused by cooling (heating) of the sample are related to the magnetic properties, which are calculated by quantum chemical methods for these structures rather than to the results of magnetometry measurements performed exclusively at low temperatures. Such studies are scarce,[198] and the most significant result is that the structures of SMMs determined at liquid nitrogen temperature can be used (in the absence of temperature-induced phase transitions) for quantum chemical calculations.[198]

A more widely used but difficult to implement approach is based on X-ray diffraction studies of the chosen SMM under different pressures.[199, 200] In these experiments, a single crystal is placed in a diamond anvil cell containing a liquid pressure transmitting medium to provide hydrostatic [201] or higher [200] pressure. Generally, the goal of these experiments is the same as that in the above-described multi-temperature studies, *i.e.*, the aim is to determine the real structures of SMMs and to use then in subsequent quantum chemical calculations of magnetic properties.[201] For example, these studies revealed a clear relationship between the zero-field splitting energy for the trigonal bipyramidal nickel(II) complex and a decrease in its trigonal

symmetry.[201] On the contrary, depending on the nature of the metal ion, an increase (or a decrease) in the barrier to magnetization reversal accompanied by the distortion of the coordination environment from the ideal pentagonal bipyramid was observed for two isostructural lanthanide complexes with increasing pressure.[199] Intermolecular interactions that are dramatically changed under the pressure applied to the crystal[199] also make an important contribution to the properties of these SMMs. For some SMMs, X-ray diffraction data under different pressures were directly related to the magnetic properties measured under different pressures.[199,201] This problem poses some technical difficulties associated with the necessity of using a diamond anvil cell; however, it makes it possible to avoid know problems with the use of quantum chemical calculations to describe systems with low-lying excited states[202] and lanthanide compounds.[199]

These studies established the relationships between the magnetic properties of SMMs and different geometric parameters (such as bond lengths, bond angles and their different combinations), which offers significant possibilities for the rational design of new SMMs, particularly, for the description of their geometry using symmetry measures.[190,199,201] The latter quantitative characterize the distortion of the coordination environment from the ideal polyhedron (for example, trigonal[201] or pentagonal[199] bipyramid) using a single parameter.[203] The larger the symmetry measure the larger the deviation of the coordination environment from the selected polyhedron and, on the contrary, the symmetry measure is equal to zero if the coordination environment completely coincides with the selected polyhedron. This approach was used, for example, to confirm the relationship between the zero-field splitting energy for the tetrahedral cobalt(II) complex[200] and the deviation of the coordination environment from the ideal tetrahedron, which is manifested in changes in the Co–X bond lengths and X–Co–X bond angles.

High-resolution X-ray diffraction studies of the electron density distribution deserves special attention. They are considered in detail in a recent review.[204] The main difference of these studies from conventional X-ray diffraction techniques, which are aimed exclusively at determining the structures of chemical compounds, is that they use high-resolution data, for example, with the diffraction angle $\theta > 50^\circ$ in the case of Mo K_α radiation, whereas the θ angle in conventional experiments is generally in the range of 26–30°. These experiments not only allow the determination of the atomic coordinates and displacement parameters[205] but also provides a unique way to obtain the complete electron density distribution in the analytical form in using the Hansen–Coppens multipole model.[206] In terms of this model, the deformation of the atomic valence shell caused by the formation of chemical bonds, which is not taken into account in the spherical atom model in conventional X-ray diffraction studies, is described by a set of multipoles (monopoles, dipoles, quadrupoles, *etc.*), the graphical analogues of which are the s, p, d, *etc.* orbitals. The populations of the corresponding multipoles for each atom are refined together with the atomic coordinates and displacement parameters (in some cases, the anharmonicity parameters of thermal motion are included) based on the X-ray diffraction data. Hence, the latter should be of high resolution. This imposes stringent requirement on the quality of the sample (the absence of disorder, twinning, significant absorption of X-rays by the crystal, *etc.*), thereby limiting the number of systems, which can be used in high-resolution X-ray diffraction experiments. However, due to growing availability of powerful laboratory and synchrotron X-ray sources and the development of new-generation detectors[183] and also the elaboration of hybrid methods,[204] high-resolution X-ray diffraction experiments are quite commonly performed[207] and provide detailed information on the nature of chemical bonding and correlated properties (including magnetic) of compounds.[208]

However, the usefulness of the data on the electron density distribution for investigations of SMMs was found quite recently[209] although high-resolution X-ray diffraction studies have immediately attracted interest from researchers dealing with single-molecule magnetism.[210] In particular, the electron density distribution of the dysprosium ion was found to be an oblate ellipsoid (Fig. 32),[211] which was predicted using the common Rinehart–Long approach.[212]

Besides, only high-resolution X-ray diffraction studies allow the experimental determination of d- and f-orbital populations of metal ions[209,211] and, correspondingly, the sequences of energy levels provided that the Aufbau principle is met.[210] This method can be used to obtain data on the electronic state of the ground state of SMMs, which is not always obvious.[33] Another advantage is that the characteristic features of the chemical bonding in crystals of SMMs can be studied[209] by examination of the electron density distribution in terms of Bader's Atoms in Molecules theory[213] based on the analysis of critical points at which the electron density gradient is equal to zero. In this case, particular attention is given to the search for bonding critical points CP(3,–1) (3 is the number of non-zero eigenvalues of the matrix of second derivatives of the electron density function, –1 is the sum of their signs) between atomic pairs. The presence of these points is a necessary condition for the existence of a chemical bonding between atoms or, in the general case, the stabilizing effect. For SMMs, this approach was used to determine interatomic interactions that affect the 3d-orbital populations of metal ions[209] or the geometry of its coordination polyhedron[214] based on the presence (in some cases, the absence) of CP(3,–1) between the corresponding atoms.[209,214] This approach was also used to evaluate the contribution of the covalent component to the metal–ligand bonding[209] based

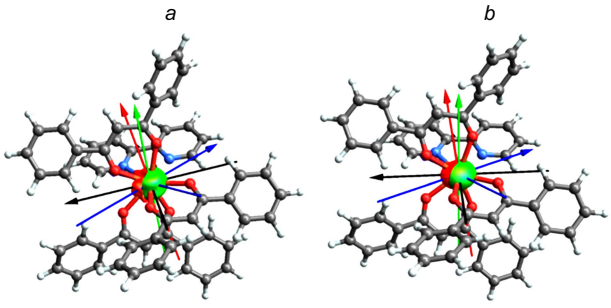


Figure 32. Electron density distribution for the dysprosium ion in the complex $Dy(dbm)_3(bpy)$ (dbm is dibenzoylmethanoate, bpy is 2,2′-bipyridine) obtained by refining the multipole populations up to the octupole level (*a*) and by refining only monopoles and quadrupoles (*b*) based on high-resolution X-ray diffraction data (red surfaces) and the structure factors calculated by a quantum chemical method (green surfaces).[211] Reproduced with the permission of Springer Nature.

on the values of the electron density and the derived functions, such as the Laplacian and the electron energy density, at CP(3, −1).[215]

However, high-resolution X-ray diffraction studies of the electron density distribution in crystals of SMMs were performed primarily in order to determine the populations of d- (Refs 33, 209, 214, 216) or f-orbitals[211] related to the electronic structure of the ground state of SMMs.[33] The multipole refinement of high-resolution X-ray diffraction data can be performed using the known approach proposed by Holladay *et al*.[217] or the specially developed method for the evaluation of f-orbital populations in SMMs[211] based on the linear transformation of the corresponding multipole parameters (quadrupoles or octupoles). Both approaches rely on the assumption that electron density on a metal ion does not have contributions of the charge transfer from the ligand; this is a reasonable assumption only for lanthanide compounds[211] that form coordination bonds primarily of ionic nature. Besides, the choice of a local system of coordinates for the metal ion on the researcher will,[33, 209, 216] which is considered as an advantage of the multipole model,[218] can lead to the ambiguity in the evaluation of its orbital populations. The latter problem is actively addressed;[211, 216] however, d-orbital populations in SMMs are used mainly to reveal the easy axis of magnetization,[211] while only average values are reported for other directions.[216]

Nevertheless, even this analysis of the electron density distribution provides a rather accuracy evaluation of d- and f-orbital populations,[211, 214] the values of which adequately (particularly, when appropriate radial functions are chosen for multipoles and the correction for the charge transfer from the ligand[214] are added) reproduce the results of high-accuracy quantum chemical calculations.[211, 214, 216] Correspondingly, these values can be used instead of the corresponding populations determined by the refinement of theoretical structure factors (the calculations of the structure factors for lanthanides compounds requires a special calculation methodology[211]) in the correlations with the zero-field splitting energy and the barrier to magnetization reversal of SMMs.[214] Although the electron density distribution can be derived from the X-ray diffraction data only in exceptional cases (particularly, for lanthanide complexes[211]), high-accuracy studies of the electron density distribution have obvious advantages over quantum chemical calculations because the electron density distribution corresponds to real crystals and, correspondingly, takes into account the relativistic effects, spin – orbit coupling and the multireference character of the wave function of SMMs.[211]

5. Conclusion

The chemical community has accumulated a wealth of experimental data on the synthesis of different d- and f-transition metal complexes. However, the magnetic properties of only a small number of compounds were investigated quite well to draw a conclusion about the prospects of their use as single-molecule magnets. It is worth noting that many recent publications contain evidence that long known and well-characterized compounds,[221 – 224] which have not been previously considered by researchers dealing with molecular magnetism, display unusual magnetic properties.[122, 189, 219, 220] First, this is due to the fact that the most common methods for investigation of single-molecule magnets are often inapplicable in chemical laboratories. Second, most of these publications were written by physicists for physicists, thereby making them difficult to understand by chemists, who are expected to address the issues of the rational design of single-molecule magnets.

The goal of this review is to partially close this gap providing (without excessive mathematical detail) answers to two main questions, which can be raised by chemists:

— what are the factors that are responsible for the single-molecule magnet properties in a particular compound

— how it can be determined?

We hope that this review will stimulate researchers in coordination and organometallic chemistry to consider the library of the previously synthesized compounds from a new side. Apparently, this will result in the design of new single-molecule magnets for the potential application in innovative devices for data storage and processing.

This review was written with the financial support of the Russian Foundation for Basic Research (Project No. 19-13-50487). The access to scientific literature was provided by the Nesmeyanov Institute of Organoelement Compounds of the Russian Academy of Sciences with the financial support from the Ministry of Science and Higher Education of the Russian Federation.

6. List of acronyms and designations

ac magnetometry — alternating magnetic field magnetometry,

CP — critical point,

DFT — density functional theory,

EPR — electron paramagnetic resonance,

FDMR — frequency domain magnetic resonance,

FIR — far-infrared spectroscopy,

Mn_{12} — manganese complex $[Mn^{III}{}_8Mn^{IV}{}_4O_{12}(MeCOO)_{16}(H_2O)_4]\cdot 2\,MeCOOH\cdot 4\,H_2O$,

NMR — nuclear magnetic resonance,

QTM — quantum tunneling of magnetization,

SMM — single-molecule magnet,

THz-EPR — terahertz electron paramagnetic resonance,

TMS — tetramethylsilane,

VSM — vibrating-sample magnetometer,

ZFC/FC experiment — experiment involving cooling in zero magnetic field (zero-field cooled, ZFC) followed by cooling in applied magnetic field (field-cooled, FC),

Designations of values:

A, B_1, B_2, C — phenomenological constants,

ΔA — differential absorption,

B — magnetic induction,

D — zero-field splitting energy,

E — total energy of the system,

g — electronic g-tensor,

H — magnetic field strength,

$\widehat{H}$ — total Hamiltonian of the system,

I — nuclear spin,

J — total angular momentum,

k — Boltzmann constant,

L — orbital momentum,

M — magnetization of the sample,

M_s — spin quantum number,

m_s — quantum number of the unpaired electron,

N_A — Avogadro s number,

$\widehat{O}_n^q$ — polynomial functions of total momentum operators,

R — gas constant,

S — total spin of the system,

s_n — spin coordinates,
T_1 — spin-lattice relaxation time,
U — energy barrier to magnetization reversal,
U_{eff} — effective barrier to magnetization reversal,
α — parameter that takes into account the number of relaxation mechanisms,
δ_{pcs} — pseudocontact shift,
δ_{cs} — contact shift,
μ_B — Bohr magneton,
μ_{eff} — effective magnetic moment,
ν — alternating magnetic field frequency,
ρ — spin density at the nucleus,
σ — set of spectroscopic constants,
τ — magnetic relaxation time,
τ^{-1} — magnetic relaxation rate,
χ — magnetic susceptibility,
χ' — in-phase component of magnetic susceptibility,
χ'' — out-of-phase component of magnetic susceptibility,
χ_m — molar magnetic susceptibility of the analyte,
ω — crystal vibration frequency.

References

1. O.Kahn. *Molecular Magnetism*. (Weinheim: VCH Publishers, 1993)
2. D.Gatteschi. *Adv. Mater.*, **6** 635 (1994)
3. R.Sessoli, D.Gatteschi, A.Caneschi, M.Novak. *Nature (London)*, **365**, 141 (1993)
4. G.Christou, D.Gatteschi, D.N.Hendrickson, R.Sessoli. *MRS Bull.*, **25**, 66 (2000)
5. J.Ferrando-Soria, J.Vallejo, M.Castellano, J.Martínez-Lillo, E.Pardo, J.Cano, I.Castro, F.Lloret, R.Ruiz-García, M.Julve. *Coord. Chem. Rev.*, **339**, 17 (2017)
6. K.Senthil Kumar, M.Ruben. *Coord. Chem. Rev.*, **346**, 176 (2017)
7. I.Castro, W.P.Barros, M.L.Calatayud, F.Lloret, N.Marino, G.De Munno, H.O.Stumpf, R.Ruiz-García, M.Julve. *Coord. Chem. Rev.*, **315**, 135 (2016)
8. J.Schnack. *Dalton Trans.*, **39**, 4677 (2010)
9. L.Bogani, A.Vindigni, R.Sessoli, D.Gatteschi. *J. Mater. Chem.*, **18**, 4750 (2008)
10. J.López-Cabrelles, S.Mañas-Valero, I.J.Vitórica-Yrezábal, P.J.Bereciartua, J.A.Rodríguez-Velamazán, J.C.Waerenborgh, B.J.C.Vieira, D.Davidovikj, P.G.Steeneken, H.S.J.van der Zant, G.Mínguez Espallargas, E.Coronado. *Nat. Chem.*, **10**, 1001 (2018)
11. E.Coronado, G.Mínguez Espallargas. *Chem. Soc. Rev.*, **42**, 1525 (2013)
12. M.A.Zykin, P.E.Kazin, M.Jansen. *Chem. – Eur. J.*, **26**, 8834 (2020)
13. A.J.Epstein, J.S.Miller. *Mol. Cryst. Liquid Cryst. Sci. Technol. Sect. A*, **228**, 99 (1993)
14. M.Cavallini, J.Gomez-Segura, D.Ruiz-Molina, M.Massi, C.Albonetti, C.Rovira, J.Veciana, F.Biscarini. *Angew. Chem., Int. Ed.*, **44**, 888 (2005)
15. D.-P.Li, T.-W.Wang, C.-H.Li, D.-S.Liu, Y.-Z.Li, X.-Z.You. *Chem. Commun.*, **46**, 2929 (2010)
16. L.Bogani, W.Wernsdorfer. *Nat. Mater.*, **7**, 179 (2008)
17. R.A.Layfield. *Organometallics*, **33**, 1084 (2014)
18. K.Liu, W.Shi, P.Cheng. *Coord. Chem. Rev.*, **289 – 290**, 74 (2015)
19. F.Pointillart, O.Cador, B.Le Guennic, L.Ouahab. *Coord. Chem. Rev.*, **346**, 150 (2017)
20. J.M.Frost, K.L.M.Harriman, M.Murugesu. *Chem. Sci.*, **7**, 2470 (2016)
21. S.G.McAdams, A.-M.Ariciu, A.K.Kostopoulos, J.P.S.Walsh, F.Tuna. *Coord. Chem. Rev.*, **346**, 216 (2017)
22. F.S.Guo, B.M.Day, Y.C.Chen, M.L.Tong, A.Mansikkamaki, R.A.Layfield. *Science*, **362**, 1400 (2018)
23. H.Andres, R.Basler, H.-U.Güdel, G.Aromí, G.Christou, H.Büttner, B.Ruffle. *J. Am. Chem. Soc.*, **122**, 12469 (2000)
24. R.Sessoli, M.Mannini, F.Pineider, A.Cornia, P.Sainctavi. In *Magnetism and Synchrotron Radiation. New Trends*. (Springer, 2010). P. 279
25. Z.Salman, R.F.Kiefl, K.H.Chow, W.A.MacFarlane, T.A.Keeler, T.J.Parolin, D.Wang. *Physica B*, **404**, 626 (2009)
26. M.Atanasov, D.Aravena, E.Suturina, E.Bill, D.Maganas, F.Neese. *Coord. Chem. Rev.*, **289**, 177 (2015)
27. D.G.R.Sessoli, A.Caneschi, M.A.Novak. *Nature (London)*, **365**, 141 (1993)
28. C.J.Milios, A.Vinslava, W.Wernsdorfer, S.Moggach, S.Parsons, S.P.Perlepes, G.Christou, E.K.Brechin. *J. Am. Chem. Soc.*, **129**, 2754 (2007)
29. S.Kang, H.Zheng, T.Liu, K.Hamachi, S.Kanegawa, K.Sugimoto, Y.Shiota, S.Hayami, M.Mito, T.Nakamura, M.Nakano, M.L.Baker, H.Nojiri, K.Yoshizawa, C.Duan, O.Sato. *Nat. Commun.*, **6**û 6503 (2015)
30. A.M.Ako, I.J.Hewitt, V.Mereacre, R.Clerac, W.Wernsdorfer, C.E.Anson, A.K.Powell. *Angew. Chem., Int. Ed.*, **45**, 4926 (2006)
31. F.Neese, D.A.Pantazis. *Faraday Discuss.*, **148**, 229 (2011)
32. N.Lis. *Acta Crystallogr., Sect. B*, **36**, 2042 (1980)
33. P.C.Bunting, M.Atanasov, E.Damgaard-Møller, M.Perfetti, I.Crassee, M.Orlita, J.Overgaard, J.Van Slageren, F.Neese, J.R.Long. *Science*, **362**, 7319 (2018)
34. M.Mostafanejad. *Int. J. Quant. Chem.*, **114**, 1495 (2014)
35. A.Abragam, B.Bleaney. *Electron Paramagnetic Resonance of Transition Ions*. (Oxford: Oxford University Press, 1970)
36. I.Waller. *Z. Phys. Hadrons Nuclei*, **79**, 370 (1932)
37. A.Abragam, B.Bleane. *Electron Paramagnetic Resonance of Transition Ions*. (Oxford: Oxford University Press, 2012)
38. S.T.Liddle, J.van Slageren. *Chem. Soc. Rev.*, **44**, 6655 (2015)
39. W.Heitler, E.Teller. *Proc. R. Soc. London, Ser. A*, **155**, 629 (1936)
40. J.Van Vleck. *Phys. Rev.*, **57**, 426 (1940)
41. H.A.Kramers. *Proc. Acad. Amsterdam Acad.*, **33**, 959 (1930)
42. Y.-C.Chen, J.-L.Liu, L.Ungur, J.Liu, Q.-W.Li, L.-F.Wang, Z.-P.Ni, L.F.Chibotaru, X.-M.Chen, M.-L.Tong. *J. Am. Chem. Soc.*, **138**, 2829 (2016)
43. M.Gregson, N.F.Chilton, A.-M.Ariciu, F.Tuna, I.F.Crowe, W.Lewis, A.J.Blake, D.Collison, E.J.McInnes, R.E.Winpenny. *Chem. Sci.*, **7**, 155 (2016)
44. B.Barbara, W.Wernsdorfer, L.Sampaio, J.Park, C.Paulsen, M.Novak, R.Ferré, D.Mailly, R.Sessoli, A.Caneschi. *J. Magn. Magn. Mater.*, **140**, 1825 (1995)
45. C.Paulsen, J.-G.Park. In *Quantum Tunneling of Magnetization – QTM'94*. (Springer, 1995). P. 189
46. J.R.Friedman, M.Sarachik, J.Tejada, R.Ziolo. *Phys. Rev. Lett.*, **76**, 3830 (1996)

47. L.Thomas, F.Lionti, R.Ballou, D.Gatteschi. *Nature (London)*, **383**, 145 (1996)
48. A.M.LaPointe. *Inorg. Chim. Acta*, **345**, 359 (2003)
49. T.Viefhaus, W.Schwarz, K.Hübler, K.Locke, J.Weidlein. *Z. Anorg. Allg. Chem.*, **627**, 715 (2001)
50. P.P.Power. *Chem. Rev.*, **112**, 3482 (2012)
51. W.A.Merrill, T.A.Stich, M.Brynda, G.J.Yeagle, J.C.Fettinger, R.D.Hont, W.M.Reiff, C.E.Schulz, R.D.Britt, P.P.Power. *J. Am. Chem. Soc.*, **131**, 12693 (2009)
52. W.M.Reiff, A.M.La Pointe, E.H.Witten. *J. Am. Chem. Soc.*, **126**, 10206 (2004)
53. W.M.Reiff, C.E.Schulz, M.-H.Whangbo, J.I.Seo, Y.S.Lee, G.R.Potratz, C.W.Spicer, G.S.Girolami. *J. Am. Chem. Soc.*, **131**, 404 (2008)
54. J.M.Zadrozny, M.Atanasov, A.M.Bryan, C.-Y.Lin, B.D.Rekken, P.P.Power, F.Neese, J.R.Long. *Chem. Sci.*, **4**, 125 (2013)
55. J.M.Zadrozny, D.J.Xiao, M.Atanasov, G.J.Long, F.Grandjean, F.Neese, J.R.Long. *Nat. Chem.*, **5**, 577 (2013)
56. H.A.Jahn, E.Teller. *Proc. R. Soc. London, Ser. A*, **161** (905), 220 (1937)
57. R.Renner. *Z. Phys.*, **92**, 172 (1934)
58. M.Atanasov, J.M.Zadrozny, J.R.Long, F.Neese. *Chem. Sci.*, **4**, 139 (2013)
59. W.Wernsdorfer, N.Aliaga-Alcalde, D.N.Hendrickson, G.Christou. *Nature (London)*, **416**, 406 (2002)
60. K.Y.Monakhov, W.Wernsdorfer. *Mendeleev Commun.*, **30**, 168 (2020)
61. D.N.Hendrickson, G.Christou, E.A.Schmitt, E.Libby, J.S.Bashkin, S.Wang, H.L.Tsai, J.B.Vincent, P.D.Boyd. *J. Am. Chem. Soc.*, **114**, 2455 (1992)
62. N.Ishikawa, S.Otsuka, Y.Kaizu. *Angew. Chem., Int. Ed.*, **44**, 731 (2005)
63. T.Fukuda, W.Kuroda, N.Ishikawa. *Chem. Commun.*, **47**, 11686 (2011)
64. Y.Horii, K.Katoh, B.K.Breedlove, M.Yamashita. *Chem. Commun.*, **53**, 8561 (2017)
65. W.Wernsdorfer, A.Caneschi, R.Sessoli, D.Gatteschi, A.Cornia, V.Villar, C.Paulsen. *Phys. Rev. Lett.*, **84**, 2965 (2000)
66. W.Wernsdorfer, S.Bhaduri, R.Tiron, D.Hendrickson, G.Christou. *Phys. Rev. Lett.*, **89**, 197201 (2002)
67. E.Colacio, J.Ruiz, E.Ruiz, E.Cremades, J.Krzystek, S.Carretta, J.Cano, T.Guidi, W.Wernsdorfer, E.K.Brechin. *Angew. Chem., Int. Ed.*, **52**, 9130 (2013)
68. J.S.Miller, J.C.Calabrese, H.Rommelmann, S.R.Chittipeddi, J.H.Zhang, W.M.Reiff, A.J.Epstein. *J. Am. Chem. Soc.*, **109**, 769 (1987)
69. J.Manriquez, G.Yee, R.S.McLean, J.Miller, A.Epstein. *Science*, **252**, 1415 (1991)
70. J.S.Miller. *Mater. Today*, **17**, 224 (2014)
71. N.Ishikawa, M.Sugita, T.Ishikawa, S.-y.Koshihara, Y.Kaizu. *J. Am. Chem. Soc.*, **125**, 8694 (2003)
72. P.-E.Car, M.Perfetti, M.Mannini, A.Favre, A.Caneschi, R.Sessoli. *Chem. Commun.*, **47**, 3751 (2011)
73. S.D.Jiang, B.W.Wang, G.Su, Z.M.Wang, S.Gao. *Angew. Chem.*, **122**, 7610 (2010)
74. K.R.Meihaus, J.D.Rinehart, J.R.Long. *Inorg. Chem.*, **50**, 8484 (2011)
75. K.Shrivastava. *Phys. Status Solidi B*, **117**, 437 (1983)
76. A.Abragam. *Principles of Nuclear Magnetism. (International Series of Monographs on Physics)*. (Oxford: Clarendon Press, 1961)
77. A.Fort, A.Rettori, J.Villain, D.Gatteschi, R.Sessoli. *Phys. Rev. Lett.*, **80**, 612 (1998)
78. R.Orbach, M.Blume. *Phys. Rev. Lett.*, **8**, 478 (1962)
79. A.Singh, K.Shrivastava. *Phys. Status Solidi B*, **95**, 273 (1979)
80. X.Feng, J.-L.Liu, K.S.Pedersen, J.Nehrkorn, A.Schnegg, K.Holldack, J.Bendix, M.Sigrist, H.Mutka, D.Samohvalov. *Chem. Commun.*, **52**, 12905 (2016)
81. J.M.Zadrozny, D.J.Xiao, J.R.Long, M.Atanasov, F.Neese, F.Grandjean, G.J.Long. *Inorg. Chem.*, **52**, 13123 (2013)
82. Y.Pontillon, A.Caneschi, D.Gatteschi, R.Sessoli, E.Ressouche, J.Schweizer, E.Lelievre-Berna. *J. Am. Chem. Soc.*, **121**, 5342 (1999)
83. M.Mannini, F.Pineider, P.Sainctavit, L.Joly, A.Fraile-Rodríguez, M.A.Arrio, C.Cartier dit Moulin, W.Wernsdorfer, A.Cornia, D.Gatteschi. *Adv. Mater.*, **21**, 167 (2009)
84. G.van der Laan, A.I.Figueroa. *Coord. Chem. Rev.*, **277**, 95 (2014)
85. L.Margheriti, D.Chiappe, M.Mannini, P.E.Car, P.Sainctavit, M.A.Arrio, F.B.de Mongeot, J.C.Cezar, F.M.Piras, A.Magnani. *Adv. Mater.*, **22**, 5488 (2010)
86. T.Lancaster, S.J.Blundell, F.L.Pratt, M.L.Brooks, J.L.Manson, E.K.Brechin, C.Cadiou, D.Low, E.J.McInnes, R.E.Winpenny. *J. Phys.: Condens. Matter*, **16**, S4563 (2004)
87. S.J.Blundell, T.Lancaster, F.L.Pratt, P.J.Baker, M.L.Brooks, C.Baines, J.L.Manson, C.P.Landee. *J. Phys. Chem. Solids*, **68**, 2039 (2007)
88. T.Lancaster, S.J.Blundell, F.L.Pratt. *Phys. Scr.*, **88**, 068506 (2013)
89. S.Carretta, J.Van Slageren, T.Guidi, E.Liviotti, C.Mondelli, D.Rovai, A.Cornia, A.Dearden, F.Carsughi, M.Affronte. *Phys. Rev. B*, **67**, 094405 (2003)
90. O.Waldmann, G.Carver, C.Dobe, D.Biner, A.Sieber, H.-U.Güdel, H.Mutka, J.Ollivier, N.Chakov. *Appl. Phys. Lett.*, **88**, 042507 (2006)
91. M.L.Baker, S.J.Blundell, N.Domingo, S.Hill. In *Molecular Nanomagnets and Related Phenomena*. (Berlin, Heidelberg: Springer, 2014). P. 231
92. E.J.McInnes. In *Single-Molecule Magnets and Related Phenomena*. (Berlin, Heidelberg, New York: Springer, 2006). P. 69
93. S.Foner. *Rev. Sci. Instrum.*, **30**, 548 (1959)
94. R.L.Carlin. *Magnetochemistry*. (Berlin, Heidelberg: Springer-Verlag, 1986)
95. H.L.Feltham, R.Clérac, L.Ungur, V.Vieru, L.F.Chibotaru, A.K.Powell, S.Brooker. *Inorg. Chem.*, **51**, 10603 (2012)
96. D.Gatteschi, R.Sessoli, J.Villain. *Molecular Nanomagnets*. (Oxford: Oxford University Press on Demand, 2006)
97. M.E.Boulon, G.Cucinotta, S.S.Liu, S.D.Jiang, L.Ungur, L.F.Chibotaru, S.Gao, R.Sessoli. *Chem. – Eur. J.*, **19**, 13726 (2013)
98. A.Chiesa, F.Cugini, R.Hussain, E.Macaluso, G.Allodi, E.Garlatti, M.Giansiracusa, C.Goodwin, F.Ortu, D.Reta. *Phys. Rev. B*, **101**, 174402 (2020)
99. A.Caneschi, D.Gatteschi, R.Sessoli, A.L.Barra, L.C.Brunel, M.Guillot. *J. Am. Chem. Soc.*, **113**, 5873 (1991)
100. J.R.Argand. *Essai sur une Manière de Représenter les Quantités Imaginaires dans les Constructions Géométriques*. (Paris: Gauthier-Villars, 1874)
101. K.S.Cole, R.H.Cole. *J. Chem. Phys.*, **9**, 341 (1941)

102. J.Krzystek, J.Telser. *Dalton Trans.*, **45**, 16751 (2016)
103. I.Nemec, R.Marx, R.Herchel, P.Neugebauer, J.van Slageren, Z.Trávníček. *Dalton Trans.*, **44**, 15014 (2015)
104. I.Nemec, R.Herchel, M.Kern, P.Neugebauer, J.van Slageren, Z.Trávníček. *Materials*, **10**, 249 (2017)
105. D.Schweinfurth, J.Krzystek, M.Atanasov, J.Klein, S.Hohloch, J.Telser, S.Demeshko, F.Meyer, F.Neese, B.Sarkar. *Inorg. Chem.*, **56**, 5253 (2017)
106. V.V.Novikov, A.A.Pavlov, A.S.Belov, A.V.Vologzhanina, A.Savitsky, Y.Z.Voloshin. *J. Phys. Chem. Lett.*, **5**, 3799 (2014)
107. J.Telser, J.Krzystek, A.Ozarowski. *J. Biol. Inorg. Chem.*, **19**, 297 (2014)
108. W.R.Hagen. *Coord. Chem. Rev.*, **190**, 209 (1999)
109. A.-L.Barra, L.-C.Brunel, D.Gatteschi, L.Pardi, R.Sessoli. *Acc. Chem. Res.*, **31**, 460 (1998)
110. B.Gorshunov, A.Volkov, I.Spektor, A.Prokhorov, A.Mukhin, M.Dressel, S.Uchida, A.Loidl. *Int. J. Infrared Millimeter Waves*, **26**, 1217 (2005)
111. M.Ozerov, B.Bernáth, D.Kamenskyi, B.Redlich, A.van der Meer, P.Christianen, H.Engelkamp, J.Maan. *App. Phys. Lett.*, **110**, 094106 (2017)
112. S.Zvyagin, M.Ozerov, E.Čižmár, D.Kamenskyi, S.Zherlitsyn, T.Herrmannsdörfer, J.Wosnitza, R.Wünsch, W.Seidel. *Rev. Sci. Instr.*, **80**, 073102 (2009)
113. S.L.Veber, S.V.Tumanov, E.Y.Fursova, O.A.Shevchenko, Y.V.Getmanov, M.A.Scheglov, V.V.Kubarev, D.A.Shevchenko, I.I.Gorbachev, T.V.Salikova. *J. Magn. Res.*, **288**, 11 (2018)
114. A.L.Barra, D.Gatteschi, R.Sessoli. *Phys. Rev. B*, **56**, 8192 (1997)
115. G.C.Brackett, P.Richards, W.Caughey. *J. Chem. Phys.*, **54**, 4383 (1971)
116. R.Won. *Nat. Photon.*, **4**, 673 (2010)
117. J.Van Slageren, S.Vongtragool, B.Gorshunov, A.Mukhin, N.Karl, J.Krzystek, J.Telser, A.Müller, C.Sangregorio, D.Gatteschi. *Phys. Chem. Chem. Phys.*, **5**, 3837 (2003)
118. Y.Rechkemmer, F.D.Breitgoff, M.Van Der Meer, M.Atanasov, M.Hakl, M.Orlita, P.Neugebauer, F.Neese, B.Sarkar, J.Van Slageren. *Nat. Commun.*, **7**, 1 (2016)
119. Y.Rechkemmer, J.E.Fischer, R.Marx, M.a.Dörfel, P.Neugebauer, S.Horvath, M.Gysler, T.Brock-Nannestad, W.Frey, M.F.Reid. *J. Am. Chem. Soc.*, **137**, 13114 (2015)
120. M.Slota, S.-D.Jiang, E Heintze, Y.Rechkemmer, M.Dressel, J.vanSlageren, L.Bogani. *Phys. Rev. B*, **99**, 134410 (2019)
121. A.A.Pavlov, D.Y.Aleshin, S.A.Savkina, A.S.Belov, N.N.Efimov, J.Nehrkorn, M.Ozerov, Y.Z.Voloshin, Y.V.Nelyubina, V.V.Novikov. *ChemPhysChem*, **20**, 1001 (2019)
122. A.A.Pavlov, J.Nehrkorn, Y.A.Pankratova, M.Ozerov, E.A.Mikhalyova, A.V.Polezhaev, Y.V.Nelyubina, V.V.Novikov. *Phys. Chem. Chem. Phys.*, **21**, 8201 (2019)
123. D.H.Moseley, S.E.Stavretis, K.Thirunavukkuarasu, M.Ozerov, Y.Cheng, L.L.Daemen, J.Ludwig, Z.Lu, D.Smirnov, C.M.Brown. *Nat. Commun.*, **9**, 1 (2018)
124. A.A.Pavlov, J.Nehrkorn, S.V.Zubkevich, M.V.Fedin, K.Holldack, A.Schnegg, V.V.Novikov. *Inorg. Chem.*, **59**, 10746 (2020)
125. E.Y.Misochko, A.V.Akimov, D.V.Korchagin, J.Nehrkorn, M.Ozerov, A.V.Palii, J.M.Clemente-Juan, S.M.Aldoshin. *Inorg. Chem.*, **58**, 16434 (2019)
126. J.Nehrkorn, K.Holldack, R.Bittl, A.Schnegg. *J. Magn. Res.*, **280**, 10 (2017)
127. J.Dreiser, A.Schnegg, K.Holldack, K.S.Pedersen, M.SchauMagnussen, J.Nehrkorn, P.Tregenna-Piggott, H.Mutka, H.Weihe, J.Bendix. *Chem. – Eur. J.*, **17**, 7492 (2011)
128. J.Nehrkorn, S.L.Veber, L.A Zhukas, V.V.Novikov, Y.V.Nelyubina, Y.Z.Voloshin, K.Holldack, S.Stoll, A.Schnegg. *Inorg. Chem.*, **57**, 15330 (2018)
129. K.S.Pedersen, J.Dreiser, H.Weihe, R.Sibille, H.V.Johannesen, M.A.Sørensen, B.E.Nielsen, M.Sigrist, H.Mutka, S.Rols. *Inorg. Chem.*, **54**, 7600 (2015)
130. J.Long, J.Rouquette, J.M.Thibaud, R.A.Ferreira, L.D.Carlos, B.Donnadieu, V.Vieru, L.F.Chibotaru, L.Konczewicz, J.Haines. *Angew. Chem., Int. Ed.*, **54**, 2236 (2015)
131. M.Kasha. *Discuss. Faraday Soc.*, **9**, 14 (1950)
132. M.Perfetti, M.Gysler, Y.Rechkemmer-Patalen, P.Zhang, H.Tastan, F.Fischer, J.Netz, W.Frey, L.W.Zimmermann, T.Schleid. *Chem. Sci.*, **10**, 2101 (2019)
133. J.Long, R.Vallat, R.A.Ferreira, L.D.Carlos, F.A.A.Paz, Y.Guari, J.Larionova. *Chem. Commun.*, **48**, 9974 (2012)
134. J.Long, E.Mamontova, V.Freitas, D.Luneau, V.Vieru, L.F.Chibotaru, R.A.Ferreira, G.Félix, Y.Guari, L.D.Carlos. *RSC Adv.*, **6**, 108810 (2016)
135. Y.Bi, C.Chen, Y.-F.Zhao, Y.-Q.Zhang, S.-D.Jiang, B.-W.Wang, J.-B.Han, J.-L.Sun, Z.-Q.Bian, Z.-M.Wang. *Chem. Sci.*, **7**, 5020 (2016)
136. R.Buchanan, K.Wickersheim, J.Pearson, G.Herrmann. *Phys. Rev.*, **159**, 245 (1967)
137. J.Long, Y.Guari, R.A.Ferreira, L.D.Carlos, J.Larionova. *Coord. Chem. Rev.*, **363**, 57 (2018)
138. O.Laporte, W.F.Meggers. *JOSA*, **11**, 459 (1925)
139. D.P.Mills, F.Moro, J.McMaster, J.Van Slageren, W.Lewis, A.J.Blake, S.T.Liddle. *Nat. Chem.*, **3**, 454 (2011)
140. W.R.Mason. In *A Practical Guide to Magnetic Circular Dichroism Spectroscopy*. (Hoboken, NJ: Wiley, 2006). P. 60
141. W.R.Mason. In *A Practical Guide to Magnetic Circular Dichroism Spectroscopy*. (Hoboken, NJ: Wiley, 2006). P. 121
142. E.A.Suturina, J.Nehrkorn, J.M.Zadrozny, J.Liu, M.Atanasov, T.Weyhermüller, D.Maganas, S.Hill, A.Schnegg, E.Bill. *Inorg. Chem.*, **56**, 3102 (2017)
143. N.Domingo, B.Williamson, J.Gómez-Segura, P.Gerbier, D.Ruiz-Molina, D.B.Amabilino, J.Veciana, J.Tejada. *Phys. Rev. B*, **69**, 052405 (2004)
144. B.Bleaney. *J. Magn. Res. (1969)*, **8**, 91 (1972)
145. C.Nitsche, G.Otting. *Prog. Nucl. Magn. Reson. Spectrosc.*, **98**, 20 (2017)
146. T.Müntener, J.Kottelat, A.Huber, D.Häussinger. *Bioconjug. Chem.*, **29**, 3344 (2018)
147. E.Ravera, G.Parigi, C.Luchinat. *J. Magn. Res.*, **306**, 173 (2019)
148. E.Ravera, G.Parigi, C.Luchinat. *J. Magn. Res.*, **282**, 154 (2017)
149. A.C.Harnden, D.Parker, N.J.Rogers. *Coord. Chem. Rev.*, **383**, 30 (2019)
150. P.K.Senanayake, N.J.Rogers, K.L.N.Finney, P.Harvey, A.M.Funk, J.I.Wilson, D.O'Hogain, R.Maxwell, D.Parker, A.M.Blamire. *Magn. Reson. Med.*, **77**, 1307 (2017)
151. O.A.Blackburn, R.M.Edkins, S.Faulkner, A.M.Kenwright, D.Parker, N.J.Rogers, S.Shuvaev. *Dalton Trans.*, **45**, 6782 (2016)

152. G.Parigi, L.Benda, E.Ravera, M.Romanelli, C.Luchinat. *J. Chem. Phys.*, **150**, 144101 (2019)
153. L.Benda, J.Mareš, E.Ravera, G.Parigi, C.Luchinat, M.Kaupp, J.Vaara. *Angew. Chem., Int. Ed.*, **55**, 14713 (2016)
154. A.Pavlov. *INEOS OPEN*, **2**, 153 (2019)
155. D.F.Evans. *J. Chem. Soc.*, 2003 (1959)
156. A.A.Pavlov, G.L.Denisov, M.A.Kiskin, Y.V.Nelyubina, V.V.Novikov. *Inorg. Chem.*, **56**, 14759 (2017)
157. C.Piguet. *J. Chem. Ed.*, **74**, 815 (1997)
158. G.A.Bain, J.F.Berry. *J. Chem. Ed.*, **85**, 532 (2008)
159. A.J.Pell, G.Pintacuda, C.P.Grey. *Prog. Nucl. Magn. Res. Spectrosc.*, **111**, 1 (2019)
160. Y.Z.Voloshin, V.V.Novikov, Y.V.Nelyubina. *RSC Adv.*, **5**, 72621 (2015)
161. J.Van Vleck. *The Theory of Electric and Magnetic Susceptibilities*. (Oxford: Oxford University Press, 1932)
162. N.Ishikawa. *Polyhedron*, **26**, 2147 (2007)
163. M.Hiller, M.Maier, H.Wadepohl, M.Enders. *Organometallics*, **35**, 1916 (2016)
164. H.Wang, K.Qian, K.Wang, Y.Bian, J.Jiang, S.Gao. *Chem. Commun.*, **47**, 9624 (2011)
165. H.Wang, T.Liu, K.Wang, C.Duan, J.Jiang. *Chem. – Eur. J.*, **18**, 7691 (2012)
166. H.Wang, B.-W.Wang, Y.Bian, S.Gao, J.Jiang. *Coord. Chem. Rev.*, **306**, 195 (2016)
167. A.Santria, A.Fuyuhiro, T.Fukuda, N.Ishikawa. *Dalton Trans.*, **48**, 7685 (2019)
168. M.Hiller, S.Krieg, N.Ishikawa, M.Enders. *Inorg. Chem.*, **56**, 15285 (2017)
169. M.Hiller, T.Sittel, H.Wadepohl, M.Enders. *Chem. – Eur. J.*, **25**, 10668 (2019)
170. V.V.Novikov, A.A.Pavlov, Y.V.Nelyubina, M.-E.Boulon, O.A.Varzatskii, Y.Z.Voloshin, R.E.Winpenny. *J. Am. Chem. Soc.*, **137**, 9792 (2015)
171. A.A.Pavlov, S.A.Savkina, A.S.Belov, Y.V.Nelyubina, N.N.Efimov, Y.Z.Voloshin, V.V.Novikov. *Inorg.Chem.*, **56**, 6943 (2017)
172. D.Y.Aleshin, A.Pavlov, S.Belova, N.Efimov, A.Belov, V.Novikov, Y.Z.Voloshin. *Russ. J. Inorg. Chem.*, **64**, 1532 (2019)
173. D.Parker, E.A.Suturina, I.Kuprov, N.F.Chilton. *Acc. Chem. Res.*, **53**, 1520 (2020)
174. H.M.McConnell. *J. Chem. Phys.*, **27**, 226 (1957)
175. E.A.Suturina, I.Kuprov. *Phys. Chem. Chem. Phys.*, **18**, 26412 (2016)
176. A.A.Pavlov, Y.V.Nelyubina, S.V.Kats, L.V.Penkova, N.N.Efimov, A.O.Dmitrienko, A.V.Vologzhanina, A.S.Belov, Y.Z.Voloshin, V.V.Novikov. *J. Phys. Chem. Lett.*, **7**, 4111 (2016)
177. V.V.Novikov, A.A.Pavlov, A.S.Belov, A.V.Vologzhanina, A.Savitsky, Y.Z.Voloshin. *J. Phys. Chem. Lett.*, **5**, 3799 (2014)
178. Y.Pankratova, D.Aleshin, I.Nikovskiy, V.Novikov, Yu.Nelyubina. *Inorg. Chem.*, **59**, 7700 (2020)
179. F.Pointillart, K.Bernot, S.Golhen, B.Le Guennic, T.Guizouarn, L.Ouahab, O.Cador. *Angew. Chem., Int. Ed.*, **127**, 1524 (2015)
180. B.A.Dougan, Z.Xue. *Sci. China, Ser. B: Chem.*, **52**, 2083 (2009)
181. E.A.Klahn, C.Gao, B.Gillon, A.Gukasov, X.Fabrèges, R.O.Piltz, S.D.Jiang, J.Overgaard. *Chem. – Eur. J.*, **24**, 16576 (2018)
182. K.Ridier, A.Mondal, C.Boilleau, O.Cador, B.Gillon, G.Chaboussant, B.Le Guennic, K.Costuas, R.Lescouëzec. *Angew. Chem., Int. Ed.*, **55**, 3963 (2016)
183. K.N.Jarzembska, R.Kamiński, L.Dobrzycki, M.K.Cyrański. *Acta Crystallogr., Sect. B*, **70**, 847 (2014)
184. P.Debye. *Ann. Phys.*, **351**, 809 (1915)
185. P.Hohenberg, W.Kohn. *Phys. Rev.*, **136**, B864 (1964)
186. Y.S.Meng, J.Xiong, M.W.Yang, Y.S.Qiao, Z.Q.Zhong, H.L.Sun, J.B.Han, T.Liu, B.W.Wang, S.Gao. *Angew. Chem., Int. Ed.*, **59**, 13037 (2020)
187. P.Shukla, K.U.Ansari, C.Gao, S.Vaidya, S.Tripathi, P.Kumar, R.J.Butcher, J.Overgaard, M.Shanmugam. *Dalton Trans.*, **49**, 10580 (2020)
188. X.-N.Yao, J.-Z.Du, Y.-Q.Zhang, X.-B.Leng, M.-W.Yang, S.-D.Jiang, Z.-X.Wang, Z.-W.Ouyang, L.Deng, B.-W.Wang. *J. Am. Chem. Soc.*, **139**, 373 (2017)
189. J.Zhang, J.Li, L.Yang, C.Yuan, Y.-Q.Zhang, Y.Song. *Inorg. Chem.*, **57**, 3903 (2018)
190. S.Gomez-Coca, E.Cremades, N.Aliaga-Alcalde, E.Ruiz. *J. Am. Chem. Soc.*, **135**, 7010 (2013)
191. E.A.Suturina, D.Maganas, E.Bill, M.Atanasov, F.Neese. *Inorg. Chem.*, **54**, 9948 (2015)
192. Y.Rechkemmer, F.D.Breitgoff, M.Van Der Meer, M.Atanasov, M.Hakl, M.Orlita, P.Neugebauer, F.Neese, B.Sarkar, J.Van Slageren. *Nat. Commun.*, **7**, 10467 (2016)
193. G.Yi, H.Cui, C.Zhang, W.Zhao, L.Chen, Y.-Q.Zhang, X.-T.Chen, Y.Song, A.Yuan. *Dalton Trans.*, **49**, 2063 (2020)
194. R.Diego, A.Pavlov, M.Darawsheh, D.Aleshin, J.Nehrkorn, Y.Nelyubina, O.Roubeau, V.Novikov, G.Aromí. *Inorg. Chem.*, **58**, 9562 (2019)
195. C.-M.Liu, D.-Q.Zhang, D.-B.Zhu. *Sci. Rep.*, **7**, 1 (2017)
196. D.Maganas, S.Sottini, P.Kyritsis, E.J.Groenen, F.Neese. *Inorg. Chem.*, **50**, 8741 (2011)
197. D.Maganas, J.Krzystek, E.Ferentinos, A.M.Whyte, N.Robertson, V.Psycharis, A.Terzis, F.Neese, P.Kyritsis. *Inorg. Chem.*, **51**, 7218 (2012)
198. K.Qian, J.J.Baldoví, S.-D.Jiang, A.Gaita-Ariño, Y.-Q.Zhang, J.Overgaard, B.-W.Wang, E.Coronado, S.Gao. *Chem. Sci.*, **6**, 4587 (2015)
199. M.S.Norre, C.Gao, S.Dey, S.K.Gupta, A.Borah, R.Murugavel, G.Rajaraman, J.Overgaard. *Inorg. Chem.*, **59**, 717 (2019)
200. A.M.Thiel, E.Damgaard-Møller, J.Overgaard. *Inorg. Chem.*, **59**, 1682 (2020)
201. G.A.Craig, A.Sarkar, C.H.Woodall, M.A.Hay, K.E.Marriott, K.V.Kamenev, S.A.Moggach, E.K.Brechin, S.Parsons, G.Rajaraman. *Chem. Sci.*, **9**, 1551 (2018)
202. D.Ganyushin, F.Neese. *J. Chem. Phys.*, **125**, 024103 (2006)
203. S.Alvarez. *Chem. Rev.*, **115**, 13447 (2015)
204. A.A.Korlyukov, Y.V.Nelyubina. *Russ. Chem. Rev.*, **88**, 677 (2019)
205. L.Aslanov, G.Fetisov, A.Loktionov, V.Markov, V.Chernyshov, S.Zhukov, A.Nesterenko, A.Chulichkov. N.Chulichkova. *Pretsizionnyi Rentgendifraktsionnyi Eksperiment. (Precision X-ray Diffraction Experiment)*. (Moscow: Moscow State University, 1989)
206. N.K.Hansen, P.Coppens. *Acta Crystallogr., Sect. A*, **34**, 909 (1978)
207. P.Coppens. *Angew. Chem., Int. Ed.*, **44**, 6810 (2005)
208. C.Gatti, P.Macchi. *Modern Charge Density Analysis*. (Dordrecht, Heidelberg, London, New York: Springer, 2012)

209. M.Craven, M.H.Nygaard, J.M.Zadrozny, J.R.Long, J.Overgaard. *Inorg. Chem.*, **57**, 6913 (2018)
210. E.Damgaard-Møller, L.Krause, J.Overgaard. In *21st Century Challenges in Chemical Crystallography II. Structure and Bonding*. Vol. 186. (Cham: Springer, 2020)
211. C.Gao, A.Genoni, S.Gao, S.Jiang, A.Soncini, J.Overgaard. *Nat. Chem.*, **12**, 213 (2020)
212. J.D.Rinehart, J.R.Long. *Chem. Sci.*, **2**, 2078 (2011)
213. R.F.W.Bader. *Atoms in Molecules: A Quantum Theory*. (Oxford: Clarendon Press, 1994)
214. E.Damgaard-Møller, L.Krause, K.Tolborg, G.Macetti, A.Genoni, J.Overgaard. *Angew. Chem., Int. Ed.*, **59**, 21203 (2020)
215. D.Cremer, E.Kraka. *Angew. Chem., Int. Ed.*, **23**, 627 (1984)
216. M.K.Thomsen, A.Nyvang, J.P.Walsh, P.C.Bunting, J.R.Long, F.Neese, M.Atanasov, A.Genoni, J.Overgaard. *Inorg. Chem.*, **58**, 3211 (2019)
217. A.Holladay, P.Leung, P.Coppens. *Acta Crystallogr., Sect. A*, **39**, 377 (1983)
218. V.Pichon-Pesme, C.Lecomte, H.Lachekar. *J. Phys. Chem.*, **99**, 6242 (1995)
219. M.Atzori, L.Tesi, E.Morra, M.Chiesa, L.Sorace, R.Sessoli. *J. Am. Chem. Soc.*, **138**, 2154 (2016)
220. S.Gómez-Coca, A.Urtizberea, E.Cremades, P.J.Alonso, A.Camón, E.Ruiz, F.Luis. *Nat. Commun*, **5**, 1 (2014)
221. S.Trofimenko. *J. Am. Chem. Soc.*, **88**, 1842 (1966)
222. J.Assour, J.Goldmacher, S.Harrison. *J. Chem. Phys.*, **43**, 159 (1965)
223. S.Trofimenko. *J. Am. Chem. Soc.*, **89**, 3170 (1967)
224. G.Bullen. *Acta Crystallogr.*, **12**, 703 (1959)